Solute Strengthening in Random Alloys

C. Varvenne, M. Leyson, M. Ghazisaeidi, W.A. Curtin

Solute Strengthening in Random Alloys

C. Varvenne[a,1], G. P. M. Leyson[b,1], M. Ghazisaeidi[c], W. A. Curtin[d,*]

[a] *Centre Interdisciplinaire des Nanosciences de Marseille, UMR 7325, Aix-Marseille Univ. - CNRS, FR-13008 Marseille, France*

[b] *Max-Planck-Institute für Eisenforschung GmbH, Düsseldorf 40237, Germany*

[c] *Department of Materials Science and Engineering, The Ohio State University, Columbus, OH, 43210,USA*

[d] *Laboratory for Multiscale Mechanics Modeling, Institute of Mechanical Engineering, École Polytechnique Fédérale de Lausanne, CH-1015 Lausanne, Switzerland*

Abstract

Random solid solution alloys are a broad class of materials that are used across the entire spectrum of engineering metals, whether as stand-alone materials (e.g. Al-5xxx alloys) or as the matrix in precipitate-strengthening materials (e.g. Ni-based superalloys). As a result, the mechanisms of, and prediction of, strengthening in solid solutions has a long history. Many concepts have been developed and important trends identified but predictive capability has remained elusive. In recent years, a new theory has been developed that builds on one historical model, the Labusch model, in important ways that lead to a well-defined model valid for random solutions with arbitrary numbers of components and compositions. The new theory uses first-principles-computed solute/dislocation interaction energies as input, from which specific predictions emerge for the yield strength and activation volume as a function of alloy composition, temperature, and strain-rate. Being a general model for materials that otherwise have a low Peierls stress, it has broad application and has been successfully applied to Al-X alloys, Mg-Al, twinning in Mg alloys, and recently fcc High-Entropy Alloys. Here, the new theory is presented in a general and systematic manner. Approximations and limiting cases that reduce the complexity and facilitate understanding are introduced, and help relate the new model to various physical features present among the historical array of models, other recent models, and simulation studies. The quantitative predictions of the model in the various materials above is then demonstrated.

Keywords: Solute Strengthening, Mechanical properties, Metallic alloys, *Ab initio* calculations, solute-dislocation interactions

1. Introduction

To facilitate the development of advanced materials, computational materials science can be used to provide guidelines for design and to give physical mechanistic insight into the origins of experimentally-derived trends. However, robust and predictive models are critical. Predictions of the macroscopic mechanical properties, such as flow stress, work hardening, and fatigue behavior, in metals or other materials undergoing dislocation-mediated plastic flow, hold particular challenges. Such behavior is controlled by phenomena at multiple scales, from atomistic through mesoscale and microstructural scales, and is associated with the collective interactions among defects (solutes, dislocations, grain boundaries, precipitates). With rapidly increasing computational power and new methods at all of these various scales, computational metallurgy is entering a new chapter where predictive capability is achievable and having an impact on the design of new materials.

Here, we present recent progress in the modeling of one broad class of materials, random solid solutions. Such materials are some of the most technologically important and/or promising materials: aluminum alloys, such as the 1xxx, 3xxx, 5xxx and solutionized 6xxx series [1] used in automotive ap-

*Corresponding author

Email address: william.curtin@epfl.ch (W. A. Curtin)

[1] C.V. and G.P.M.L. equally contributed to this article.

plications, austenitic stainless steels [2], many binary alloys such as Ni-Fe and Cu-Ni [3, 4], and the emerging high entropy alloys (HEAs) [5, 6, 7]. Many precipitation-strengthened alloys also retain some solid solution strengthening that is not negligible. Interstitial solutes, such as hydrogen, carbon, and nitrogen, also confer strengthening that may be beneficial or detrimental, and their high mobility can contribute to dynamic strengthening phenomena.

In the next section, we briefly discuss the main historical concepts that developed over many decades. In subsequent sections, we present the current model framework in general. We then show how the current model encompasses some historical models, in terms of general scaling of strengthening versus material parameters, so that the current model can be seen as a holistic version of the historical models but with precise and computable material parameters. We also note connections to other recent models when pertinent. We then present applications of the model to a sequence of cases, each of which reveals some new features in the solute strengthening that arise naturally from the model due to the different dislocation structures in each case.

2. Background

Solute strengthening arises from the interaction of a dislocation with the solutes in the lattice. These interactions fall into two basic categories: those where the solute changes or reconfigures the dislocation core structure and those where the solute leaves the topology of the core structure largely intact. When a solute changes the core structure, the strengthening effects depend on the specific details of the interaction and how the core structure is changed [8, 9, 10, 11]. We do not envision any general theory for this important class of problems; presumably the changes in structure and associated energies are very specific to the solute, the matrix, and the dislocation character. When a solute distorts the core but does not change it topologically, and/or when solutes outside the core interact through nominally elastic interactions, then a general theory can be developed, and that is the focus of the work presented here.

When solutes do not change the core structure, the fundamental quantity is the interaction energy $U(x_i, y_j, z_k)$ between a straight dislocation at the origin with line direction z and glide direction x, and a solute at position (x_i, y_j, z_k). At the simplest level, this interaction energy can be modeled as the mechanical interaction energy between the straight dislocation pressure field $p(x_i, y_j)$ and the misfit volume ΔV of the solute with respect to the matrix material. This interaction energy $U_{el}(x_i, y_j) = -p(x_i, y_j)\Delta V$, also referred to as the first order "size" interaction [12], is equal to the work done on the dislocation pressure field by the expansion or contraction of the material upon addition of the misfitting solute atom. This mechanical interaction energy can be generalized to include the interaction energy between deviatoric misfit strains and the deviatoric dislocation stress field (the first order "shape" interaction), which is typically important for interstitial solutes [13, 14, 15]. For simplicity here, we focus on misfit volumetric strains that are appropriate for substitutional solutes in cubic matrices [16, 17]. The elastic interactions are long-ranged, since the dislocation stress field decays only as $1/r$ with distance r from the center of the dislocation, and give a quantitative description of the solute/dislocation interaction away from immediate dislocation core region [13, 14, 15, 16, 17, 18].

When the solute is located within the core region of the dislocation, *i.e.* along the glide plane and within the highly-distorted region of the core, additional effects between the solute and the dislocation can occur. Part of the chemical short-range interaction can be estimated using additional elasticity models. Since the addition of solutes changes the elastic moduli of the material, a solute atom can be envisioned to possess elastic constants that differ from the host matrix, giving rise to an "elastic inhomogeneity" interaction energy [12, 19, 20]. This interaction decays as $1/r^2$ so is short-ranged and, within linear elasticity, can be simply added to the first-order size interaction. A "second order size" interaction arises when non-linear effects (e.g. third-order elastic constants) are considered, and also contributes at short range [12]. However, both concepts are of limited practical utility because it is difficult to define the "elastic constants" of a solute and to deal with non-linear elasticity. Another "chemical" core-specific interaction is associated with solute/stacking-fault interactions [21], arising for dislocations having a dissociated core consisting of two partials separated by a stacking fault ribbon, as occurs in fcc and many slip systems of hcp materials. This interaction will be discussed in section 4.3.

With the advent of high-performance comput-

ing, and efficient techniques to deal with the long-range elastic fields of dislocations [22, 23, 24], it is now possible to compute dislocation core structures using first-principles methods, most commonly using Density Functional Theory (DFT). This topic is covered in depth in the partner Overview Article "*Ab initio* modeling of dislocation core properties" [25]. Using the same methods, the solute/dislocation interaction energies $U(x_i, y_j)$ for any solute at atomic positions $\{x_i, y_j\}$ in and around a dislocation core in any matrix can be computed directly. While computationally demanding, it provides the fundamental information (the interaction energy) including all "chemistry" and short-range effects at the highest level of fidelity available at the present time. Due to their value, such computations have been undertaken for a number of solutes in a number of matrix materials, primarily for edge dislocations and mainly at atomic sites just on either side of the glide plane and within the partial dislocations of dissociated cores, where "chemistry" effects are expected to be most important and where elasticity is most likely to fail. For solutes away from the core region, e.g. the elastic interaction energy $U_{el}(x_i, y_j) = -p(x_i, y_j)\Delta V$ is used, with ΔV computed by first-principles and with the dislocation pressure field $p(x_i, y_j)$ computed using the first-principles-computed core structure. The pressure field can be computed using local elastic strains and elastic moduli or by using the computed distribution of Burgers vector along the glide plane within a Peierls-Nabarro-type model [18, 26]. Thus, both near-core and far-field interaction energies are computed on the same underlying dislocation structure and solute/matrix chemistry. Figure 1 shows the resulting interaction energies $U(x_i, y_j)$ for several cases that will be studied here. We note in particular that the interaction energies, calculated directly by DFT in some regions and via elasticity in others, are quite continuous, indicating the accuracy of the elasticity model rather close to the core, but still in a region where the local atomic environment is that of the distorted crystal lattice. This continuity also shows that the near-core energies are not significantly larger than those at slightly further distances, immediately suggesting that both near-core and far-field interactions might contribute comparably to the net strengthening.

The above discussion focuses on solute/dislocation interaction energies. A number of historical models have been developed based on the forces exerted by solutes on dislocations. The force of a solute on a straight dislocation can be computed as a configurational force derived from the interaction energy. Specifically, the force exerted by the solute in the glide direction x can be computed, in a continous formulation, as $F(x, y) = -dU(x, y)/dx$, *i.e.* it is the change in interaction energy as the relative position of the solute and the dislocation changes. Both energetic and force-based concepts capture the same basic physics and, while the theoretical paths appear rather different, the final outcomes should be the same aside from approximations made along each path. We will focus below on an energy-based approach.

Whether the long-range or short-range interactions control the strength has given rise, historically, to two broad competing theories for solute strengthening. The strong-pinning theory (Friedel [27], Fleischer [28, 29]) considers only solute atoms in the glide plane(s) of the dislocation and treats them as independent point obstacles that pin the dislocation. The solutes are characterized by $F_{\max}$, the maximum resistive force exerted by the solute on the dislocation. Under stress, the dislocation bows out in the regions between the solutes, exerting forces that counteract resisting forces of the solutes. The zero-temperature yield stress for this Friedel mechanism, τ_{y0}^F, is the stress at which the curved dislocation exerts a force on the dislocation segment at the solute that is sufficient to overcome the resistive force of the solute. The Friedel strength for a random distribution of solutes at concentration c is given by

$$\tau_{y0}^F = \left(\frac{F_{\max}}{2\Gamma}\right)^{\frac{3}{2}} \left(\frac{2\Gamma}{b^2}\right) c^{\frac{1}{2}}. \quad (1)$$

where Γ is the dislocation line tension that relates the dislocation bow out to the force exerted on the obstacle, and b is the magnitude of the Burgers vector.

Examining Fig. 1, it is clear that solute forces are generated at many positions in and around the dislocation core, even if attention is confined to only the planes above and below the glide plane. The basic Friedel model neglects all such complications. Recognizing that many solutes can simultaneously exert forces on the dislocation, the weak-pinning model (Mott-Nabarro [30], Mott [31], Labusch [32, 33]) considers the collective interaction of the random solutes with the dislocation. Strengthening is then attributed to the occurrence

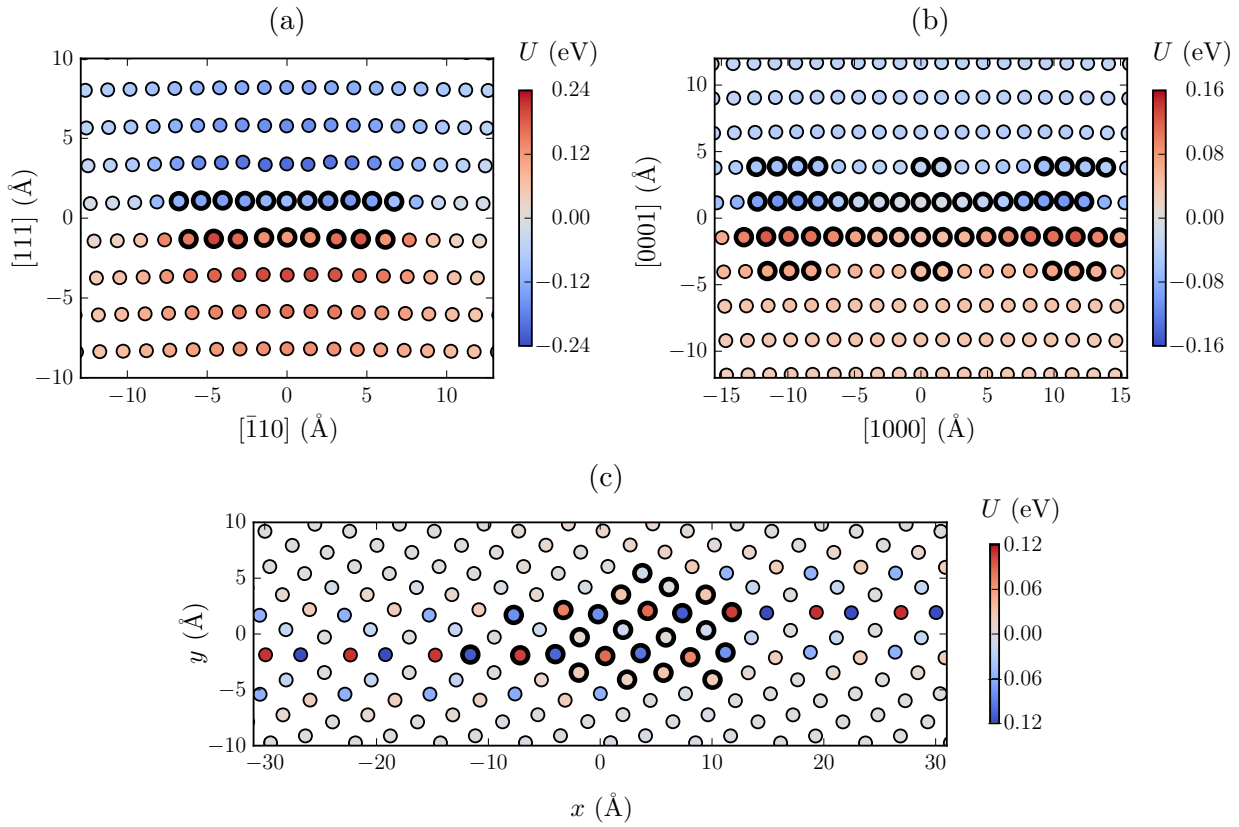

Figure 1: Solute/dislocation interation energy $U(x_i, y_j)$ versus solute position (x_i, y_j, z_k) for various materials and solutes; (a) Mn solutes around Al edge dislocation, (b) Zn solutes around Mg basal edge dislocation and (c) Al solutes around Mg twin edge dislocation on a twin boundary. Sites indicated by bold symbols are computed using DFT and all other sites are computed using the elastic contribution to the interaction energy. The core structure is optimized in DFT calculations using the Lattice Green's Function method [22].

of favorable statistical fluctuations in the overall solute configuration that locally bind the dislocation much more strongly than any individual solute. Labusch first considered only solutes in the glide plane, although the concept is really three-dimensional in nature. He then derived a zero-temperature flow stress τ_{y0}^L that uses many of the same parameters as the Friedel model, plus a parameter w that represents the spatial range of interaction of the solutes with the dislocation (and discussed further below). The resulting zero-temperature Labusch strength is

$$\tau_{y0}^L = \left(\frac{F_{\max}^4 w}{4\Gamma b^7}\right)^{\frac{1}{3}} c^{\frac{2}{3}}. \tag{2}$$

which shows a different scaling with solute concentration c as compared to Friedel's model.

At any given solute concentration, the operative mechanism has historically been assumed to be the mechanism that gives the strongest zero-temperature yield stress. Taking the ratio of Eqs. (1) and (2) yields $\beta^{1/6}$ where β is the transition parameter first identified by Labusch [32, 33] as

$$\beta = \frac{F_{\max} b^2}{4\Gamma c w^2}. \tag{3}$$

When $\beta \gg 1$, the strong-pinning model gives a much larger zero-temperature yield stress and is expected to be the dominant mechanism. Conversely, the weak-pinning model is dominant when $\beta \ll 1$. There is thus a transition concentration c_0^{trans} at $\beta = 1$, $c_0^{\text{trans}} = \frac{F_{\max} b^2}{4\Gamma w^2}$. At low concentrations $c \ll c_0^{\text{trans}}$, the strong pinning mechanism is dominant and at high concentrations $c \gg c_0^{\text{trans}}$ the weak

pinning mechanism is dominant. Using typical materials parameters gives a transition concentration $\sim 10^{-2}$, which has led to the *assumption* that the strong pinning model is applicable at moderate to low solute concentrations [32, 34].

Solute strengthening is, of course, temperature- and strain-rate-dependent, *i.e.* the underlying process is thermally-activated[2]. The standard Labusch and Friedel theories are zero-temperature theories. Extending the theories to finite temperatures, *i.e.* examining the energy barriers to dislocation motion, reveals a significant difference between the two theories. The energy scale of the Friedel model is the maximum interaction energy $U_{\max}$ of a single solute with the straight dislocation, independent of solute concentration [18]. As seen in Fig. 1, this energy is typically on the order of $\sim 100 - 200$ meV. Applied stresses reduce the barrier toward zero as the stresses approach the zero-temperature yield stress. Therefore, the energy barrier for thermally-activated escape of the dislocation across a single pinning solute is very low, and the escape rate very fast, at moderate temperatures (with $kT \sim$ 25 meV at room temperature). Correspondingly, the finite-temperature yield stress decreases rapidly with temperature, and simple models show that the Friedel mechanism has a characteristic temperature $T_\circ^F \sim$ 100–200 K at which the strength is essentially zero. In contrast, the energy scale of the Labusch model is related to the collective solute fluctuations and scales as $\sim c^{1/3}$, and can be much greater than $U_{\max}$ even at moderately low concentrations ($c > 10^{-4}$). The yield stress of the Labusch model thus decreases much more slowly with increasing temperature as compared to the Friedel model (and also never goes to zero; see discussion below). At finite temperature, the concentration at which there is a transition from the Friedel to the Labusch model, c^{trans}, is then much smaller than the zero-temperature estimate c_0^{trans}. Detailed estimates show, for example, that $c^{\text{trans}} < 10^{-4}$ when $T > 78$ K for the Al-X (X= Mg, Si, Cu, Cr, Mn and Fe) and the Mg-Al (basal) systems [36]. As a result, the Friedel model rarely applies for moderate solute/dislocation binding energies. For solutes that change the core structure, and with much larger associated interaction energies (e.g. $U_{\max} = 1$ eV [8]), the Friedel model may become pertinent [27, 32] because the core-changing solutes dominate over all other solute interactions in the far-field and the activation energy barrier is significant.

Both strong-pinning and weak-pinning models struggle to deal quantitatively with both the long-range interactions and the short-range interactions. The Friedel-type models entirely neglect the long-range interactions, so that even solutes just two atomic planes above or below the glide plane are not considered to exert forces on the dislocation even though their maximum pinning force can be appreciable [37]. If such solutes were included, the Friedel theory would need to include different values for $F_{\max}$ for each atomic plane and, moreover, the "spacing" between solutes would become very small so that the dislocation bow out would be occurring over atomic distances where the line tension model surely fails. The early Labusch model, and recent derivations of the weak-pinning model [20], also considered solutes only near the glide plane. In this limit, the interaction energy falls off rapidly ($1/d^2$) with distance d along the glide plane, so that the concept of a finite range w is acceptable. However, when extended to 3D (*i.e.* not just solutes on the glide planes), the Labusch model must also ignore long-range interactions beyond a certain distance. Since the solute/dislocation interactions decay only as $1/r$, fluctuations in the net positive and negative interactions scale as $1/r^2$, and the integral of those fluctuations over a cylinder of radius R around the dislocation line diverges as $\ln(R)$. To avoid this problem, the Labusch model has traditionally adopted the 2d concept by invoking a cut-off in the interaction energies at an arbitrary distance w. Unfortunately, all predictions depend on the undefinable w, while attempts to "measure" a w from the solute/dislocation interaction forces in atomistic simulations [38] cannot be quantitative because of the fundamental $1/r$ scaling of the interaction energy. With respect to short-range interactions, researchers had little detail about the true dislocation core structures. So, a singular Volterra field associated with a sharp dislocation core was typically used, and the short-range interactions were simply cut off at some convenient but ill-defined distance. Argon [20], for example, ignores solutes in the two planes immediately above and below the glide plane, denoting this a "dead zone", even though this is precisely where the interaction energies and forces are the largest (see Fig. 1), and considers only the planes just above and below these planes. In general, the theories

[2] We do not consider here the dynamic overshoot and possible quantum effects that can occur at very low temperatures $T < 50K$ [20, 35].

make uncontrolled approximations precisely where the solutes will have the largest effects.

The short-range issue is resolved, in principle, by the detailed computations of solute/dislocation interaction energies as shown, for example, in Fig. 1. How this more-detailed information can be embedded into the historical models has not been addressed. For purposes of guiding alloy design, *i.e.* selection of solutes, Trinkle *et al.* [39] devised two quantitative measures for the solute/dislocation interaction energy, a misfit volume parameter and a solute/stacking fault interaction parameter, and used these parameters in Fleischer/Friedel-type model to predict trends in solute strengthening at 0 K. Quantitatively predictive models have remained elusive, however. The long-range issue was only clearly addressed by the new theory presented in the following sections. An inkling of the resolution of the divergence problem at long-range can be found, however, in the study of the so-called Cottrell atmosphere formed by solutes diffusing around a fixed dislocation. Hirth *et al.* [40] showed that, although the energy of the solute-cloud/dislocation diverges (infinite binding of the dislocation), the stress to move the dislocation does not diverge. The stress does not diverge because the (diverging) energy contributions of solutes far from the dislocation do not affect the net configurational force $-dU(x,y)/dx$ upon incremental motion of the dislocation. A similar feature will emerge here in solute strengthening with no diffusive motion of the solutes, *i.e.* a dislocation moving through a *fixed* field of randomly-distributed solutes, leading to a convergent theory.

Experimentally, there are many excellent data sets on the yield strength versus temperature and/or strain-rate in binary fcc alloys, mainly with a dilute ($< 1\%$) concentration of one type of solute [29, 41, 42, 43, 44, 45, 46, 47, 48]. These experiments clearly show a commonality in the flow behavior versus temperature and versus concentration. Moreover, experiments have measured the apparent activation volume $V \sim (1/kT)d(\ln\sigma)/d\ln\dot{\varepsilon}$, which reveals the underlying length scale of dislocation motion during whatever thermally-activated process is controlling the flow behavior [44, 49, 50]. At the dislocation level, the activation volume can be expressed as the derivative of the stress-dependent energy barrier versus stress, $V = -d\Delta E(\tau)/d\tau$, and so directly connects to quantities arising in any theory. Moreover, Basinski postulated the "stress equivalency" principle: if two different alloys have the same yield stress at the same temperature and strain-rate then they will have the same activation volume, regardless of the types of solutes or their concentrations [44, 50]. The "stress equivalency" principle has been demonstrated experimentally many times.

With a strong empirical data base, the historical theories have been applied to predict qualitative and quantitative trends. Nabarro showed that some features related to stress equivalency emerge naturally from the Labusch-type models, solidifying the broad applicability of the Labusch model, consistent with our discussion above. Earlier, Kratchovil and Neradova [43] showed that the (extrapolated) zero-temperature strength scales with solute concentration as $c^{2/3}$, as predicted by the Labusch model. Nonetheless, the simplicity of the Friedel model - it contains just a few physically-based parameters - has led to continued applications of the model concepts. In particular, when the Friedel model based on pinning by individual solute atoms has failed to quantitatively explain experiments, researchers have postulated the existence of solute "clusters" as the operative pinning points within a Friedel-type model [51, 52, 53]. These experiments are, however, well-interpreted in terms of the Labusch-type models. The Labusch-type models (*i.e.* models that consider the collective statistical fluctuations of the random solutes as causing the pinning) have thus, in general, provided a framework for qualitative interpretation of many experiments, in spite of nagging theoretical issues. Quantitatively, however, the models are not accurate, which is not surprising given the approximations, particularly for the interaction energies. Argon shows that the estimated $F_{\max}$ parameter in the Labusch model is 2-3 times larger than the value derived by fitting theory to experimental data, so that the model has limited predictive capability. Versions of the Labusch model have attempted to describe experiments using very simplified forms, such as $\tau_y = K\sum_n c_n^{2/3}\Delta V_n^{4/3}$, with n referring to the elements in solid solution and with K being a fitting parameter [54, 55], without any regard for the temperature and strain-rate dependence of the flow stress.

Finally, experimental data on some systems shows a high-temperature "plateau", *i.e.* the yield stress becomes less temperature-dependent than expected based on the models. "Plateau" stresses have a long history and are usually attributed to

"athermal" mechanisms, such as long-range dislocation/dislocation interactions [56]. "Athermal" mechanisms are those with large energy barriers but also large length scales, for which the strength is not high but the barrier renders that strength temperature-insensitive. In solute-strengthened materials, the "plateau" is, however, dependent on solute concentration itself. The mechanistic origins of such plateaus have historically been unknown. Labusch [57, 58] suggested that additional energy barriers enter at high temperatures, but without substantial quantification. Zaiser [59] used scaling arguments coming from the theory of flux pinning in superconductors and provided a clearer picture of how the "plateau" arises and its connection to the low-temperature solute strengthening. Discussion of the physical origin(s) of such "plateaus", based on the progress resulting from the recent development, is presented below.

In this Overview, we present a new Labusch-type solute strengthening model that resolves many of the conceptual and operational difficulties of the historical models. The derivation of the Labusch-type model is quite different from previous derivations, although with similarities to the analysis of Zaiser [59]. The analysis provides a clean, physical, and energy-based picture of how a dislocation moves through a random field of solutes. The theory starts from the solute/dislocation interaction energies and proceeds forward with a few non-critical assumptions. The resulting model is parameter-free and generally applicable across materials and crystal structures, and interfaces (twinning). To date, the theory has only been applied to cases with very low intrinsic Peierls stresses where the solute strengthening dominates the flow stress. The new theory reproduces all the positive features of the Labusch-type models, and the final functional forms for flow stresses and energy barriers are consistent with historical models. However, the coefficients emerge directly from the solute/dislocation interaction energies, making the model predictive. By examing limiting cases of the model, we can also make specific contact with the various historical models and concepts.

3. Theory of Solute Strengthening

In this section, a general theory of solute strengthening in substitutional alloys with arbitrary number of components and arbitrary composition is described. The presentation considers fcc crystals, but most aspects of the theory are more general. Basic concepts and physical mechanisms responsible for the strengthening are first introduced, and then the full theory leading to the temperature, strain-rate and compositional dependance of the strength is derived.

3.1. Average matrix in a random alloy

We consider an N-component random solid solution alloy, with concentration c_n of the n^{th} element, satisfying the sum rule $\sum_{n=1}^{N} c_n = 1$. Except in the case of dilute alloys, there is no specific reason to identify one specific elemental component as the matrix, *i.e.* as the reference state for the real material. Indeed, when the concentrations of alloying elements are non-dilute, there is not one major element nor can the real solid solution be considered as a small perturbation of the matrix of one of the elements. Rather, an effective matrix at the overall alloy composition can be envisioned, which has the crystal structure of the real solid solution alloy. Such an average alloy reference state can be demonstrated explicitly for systems represented by Embedded Atom Method (EAM) interatomic potentials [60, 61], for instance, and an average alloy is the basis of effective medium approaches and coherent potential approximations in electronic structure theory [62, 63, 64]. The effective matrix material has all of the important *average* properties of the true random alloy: lattice constant a, elastic constants $\{C_{ij}\}$ including shear modulus μ and Poisson's ratio ν, and stable/unstable stacking fault energies $\gamma_{\rm SF}$ and $\gamma_{\rm USF}$. All of these quantities depend on the alloy composition, but are well-defined average quantities. The gliding dislocations in an effective fcc matrix would be the typical $\{111\}\langle 110\rangle$ dislocations, with a Burgers vector $\boldsymbol{b} = a/2\langle 110\rangle$, dissociation into two Shockley partials separated by an intrinsic stacking fault, and glide at very low Peierls stresses [20, 56, 65, 66]. Standard results for dilute systems, where the average matrix approaches that matrix of the dominant element of the alloy, emerge naturally when the concentration of one alloy component approaches 1 while the other concentrations approach zero.

Within the average matrix material, each elemental alloy atom can be viewed as a "solute" atom embedded into the average "matrix" of the surrounding material [61, 65]. Each solute of type n has some average properties in the average matrix, such as a misfit volume $\Delta\overline{V}_n$. In the true

random alloy, each specific solute atom has a misfit volume that depends on the precise surrounding distribution of other atoms, and can be represented as the average value plus a fluctuating term, $\Delta V_n(x_i, y_j, z_k) = \Delta\overline{V}_n + \delta V_n(x_i, y_j, z_k)$. The average misfit volume can be determined, for instance, by measuring the change in atomic volume $\overline{V}$ versus alloy composition, and taking the appropriate derivatives as

$$\Delta\overline{V}_n = \sum_m c_m \left[\left.\frac{\partial\overline{V}}{\partial c_n}\right|_{\bar{c}} - \left.\frac{\partial\overline{V}}{\partial c_m}\right|_{\bar{c}} \right]. \quad (4)$$

These average misfit volumes follow the sum rule $\sum_n c_n \Delta\overline{V}_n = 0$, since the reference state is the stress-free average material at average lattice constant a. Each solute will also interact with any structural defect in the effective matrix material. For a straight dislocation in the average matrix, centered at the origin and lying along the z direction, an individual solute atom of type n at position (x_i, y_j, z_k) has an interaction energy with the dislocation of $U^n(x_i, y_j, z_k) = \overline{U}^n(x_i, y_j)$ independent of z because the straight dislocation in the average matrix is periodic along z, as shown schematically in Fig. 2b. In the true random alloy, a solute of type n at position (x_i, y_j, z_k) has a specific interaction energy $U^n(x_i, y_j, z_k)$ due to the specific local distribution of other solutes around (x_i, y_j, z_k). For a statistical distribution of local environments, the true interaction energy can thus be expressed as the average value in the average matrix plus a fluctuation, $U^n(x_i, y_j, z_k) = \overline{U}^n(x_i, y_j) + \delta U^n(x_i, y_j, z_k)$. If the interaction was purely elastic, then the average interaction energy would be directly related to the average of the solute misfit volume through the pressure field of the dislocation in the average matrix. The additional fluctuations $\delta U^n(x_i, y_j, z_k)$ in the interaction energy of the real random alloy would be related to the fluctuations in both the misfit volume $\delta V_n(x_i, y_j, z_k)$ and the misfit solute shape (deviatoric misfit strains) since the average solute shape contribution is zero, by symmetry, in a cubic matrix. The interaction energy $U^n(x_i, y_j, z_k) = \overline{U}^n(x_i, y_j) + \delta U^n(x_i, y_j, z_k)$ including both the interaction in the average matrix material and the additional fluctuations is the fundamental input to the theory for solute strengthening. In the dilute limit, where one element acts as the matrix, $U^n(x_i, y_j, z_k) = \overline{U}^n(x_i, y_j)$, independent of z_k, and can be computed as shown in Fig. 2b. For non-dilute systems, computation of $U^n(x_i, y_j, z_k)$ or $\overline{U}^n(x_i, y_j)$ is challenging, but their existence is clear.

3.2. Energy of a straight dislocation segment in a random alloy

Strengthening, *i.e.* increased stress required to move a dislocation due to the presence of solutes, arises from the totality of the interaction energies between all of the solutes and each individual dislocation. The average matrix concept allows us to imagine a straight dislocation in that matrix, with surrounding solutes. The random distribution of solutes in the lattice gives rise to local fluctuations in solute concentrations and lattice distortions. The dislocation is thus attracted to some fluctuations and repelled by others. A key concept in the model is the energy *change* of a straight dislocation segment of length ζ when the dislocation glides a distance w from an initial position at $x = 0$. The change in the position of the dislocation relative to the positions of the (fixed) solutes leads to a potential energy change of

$$\Delta U_{tot}(\zeta, w) = \sum_{\substack{i,j,k \\ n}} s^n_{ijk} \left[U^n(x_i - w, y_j, z_k) - U^n(x_i, y_j, z_k) \right], \quad (5)$$

where $s^n_{ijk} = 1$ if a type-n solute is at position (x_i, y_j, z_k) and 0 otherwise. This energy change can be positive or negative, and has a statistical distribution. We are interested in those environments that pin the dislocation segment (*i.e.* lower the system energy). The typical energy reduction associated with such favorable "binding" environments is the negative (binding taken as a negative energy) of the standard deviation of the energy change

$$\sigma_{\Delta U_{\rm tot}}(\zeta, w) = \left[\left\langle \Delta U^2_{\rm tot}(\zeta, w) \right\rangle - \left\langle \Delta U_{\rm tot}(\zeta, w) \right\rangle^2 \right]^{\frac{1}{2}}. \quad (6)$$

Because the solutes are randomly distributed, *i.e.* uncorrelated (no short range order), the quantity $\sigma_{\Delta U_{\rm tot}}(\zeta, w)$ can be computed analytically. Invariance of the dislocation along z allows the average over the variations $\delta U^n(x_i, y_j, z_k)$ due to local distortions and/or local chemical environment among the sites z_k to be rigorously performed [61], leading to

$$\sigma_{\Delta U_{\rm tot}}(\zeta, w) = \left(\frac{\zeta}{\sqrt{3}b} \right)^{\frac{1}{2}} \Delta\tilde{E}_p(w), \quad (7)$$

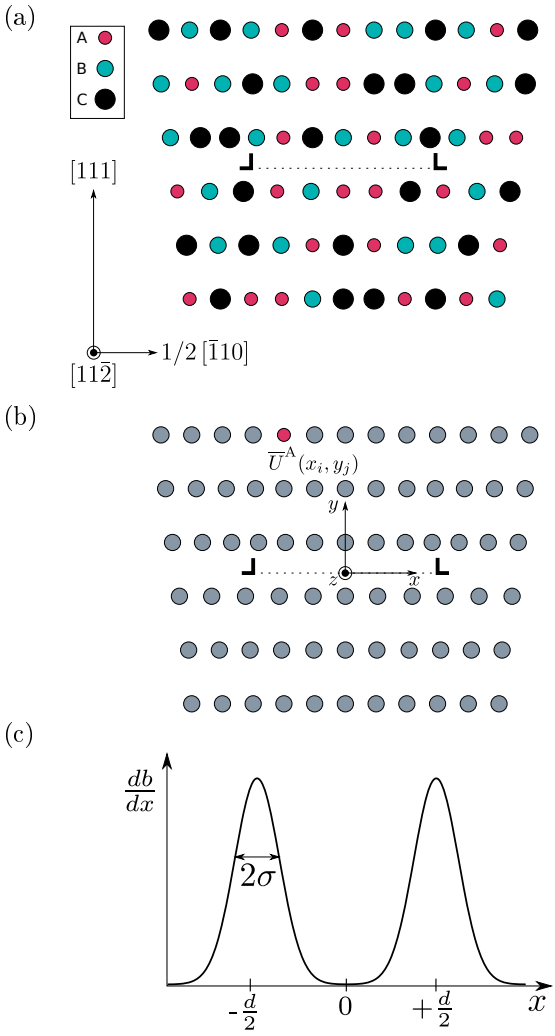

Figure 2: Effective medium approach for dislocation/solute interactions: (a) Fully-random 3-component alloy containing a dissociated edge dislocation; (b) Effective matrix material of the same alloy, with an embedded A "solute" at position (x_i, y_j, z_k) relative to the dislocation centered at the origin, with interaction energy $\overline{U}^{A}(x_i, y_j)$; (c), Normalized Burgers vector distribution $\frac{db}{dx} \sim e^{-\frac{1}{2}\left(\frac{x-d/2}{\sigma}\right)^2} + e^{-\frac{1}{2}\left(\frac{x+d/2}{\sigma}\right)^2}$ along the glide plane of edge dislocation in the effective matrix, with d the dislocation dissociation distance and σ describing the partial spreading.

with

$$\Delta\tilde{E}_p(w) = \left[\sum_{\substack{i,j \\ n}} c_n\left(\Delta\overline{U}^n_{ij}(w)^2 + \sigma^2_{\Delta U^n_{ij}}\right)\right]^{\frac{1}{2}}, \qquad (8)$$

where $\Delta\overline{U}^n_{ij}(w) = \overline{U}^n(x_i - w, y_j) - \overline{U}^n(x_i, y_j)$ and $\sigma_{\Delta U^n_{ij}}$ is the associated standard deviation of the distribution due to local fluctuations. $\Delta\tilde{E}_p(w)$ is the key mesoscale quantity for strengthening in the theory. We note that this quantity includes the additional fluctuations in interaction energy that arise in the true random alloy within the framework of the effective matrix.

The computation of $\Delta\tilde{E}_p(w)$ does not represent any convergence issues. The energy *difference* $\Delta\overline{U}^n_{ij}(w)$ due to solutes far from the dislocation, *i.e.* where $r >> w$ with $r = (x_i^2 + y_j^2)^{1/2}$, scales as w/r^2 and so the sum over all sites $\{i, j\}$ in Eq. (8) is convergent. As long as w emerges as a finite distance (see below), there is no divergence in the sum. The quantity w is not a cut-off distance in any way, and thus has a very different meaning than that arising in the original Labusch model.

3.3. Minimum energy configuration of a long dislocation in a random alloy

We have seen that straight dislocation segments can lower their energies by moving to favorable solute fluctuations that exist in the random alloy. However, different segments along a long dislocation line will want to move to different positions along the glide plane, *i.e.* the dislocation will not remain straight, and there is an elastic energy cost to creating the non-straight dislocation. Therefore, an initially straight dislocation of length L can minimize its total energy by adopting a wavy configuration where segments of some characteristic length ζ_c reside in regions of favorable fluctuations. These segments lie at the minima in a potential energy landscape having typical minima and maxima spaced by some characteristic distance w_c along the glide plane. The pinned segments ζ_c are connected through additional segments of length ζ_c to create a wavy, quasi-sinusoidal configuration (see Fig. 3). Adopting such a wavy configuration involves bowing of the dislocation, which has the elastic energy cost associated with the dislocation "line tension" Γ. For the configuration envisioned here, the cost of bowing is related to the change in total length of the dislocation and is given by

$\Delta E_{\rm LT}(\zeta_c, w_c) = \Gamma w_c^2/2\zeta_c$ per $2\zeta_c$ dislocation portion (see Fig. 3) when $w_c \ll \zeta_c$ (verified ex post facto).

To determine the characteristic ζ_c and w_c, we consider all possible dislocation configurations ζ, w and minimize the total energy with respect to ζ and w. The total energy of a wavy dislocation is the sum of the elastic energy penalty of bowing and of the potential energy gain of favorable solute environments,

$$\Delta E_{\rm tot}(\zeta, w) = \left[\Gamma\frac{w^2}{2\zeta} - \left(\frac{\zeta}{\sqrt{3}b}\right)^{\frac{1}{2}}\Delta\tilde{E}_p(w)\right]\left(\frac{L}{2\zeta}\right), \tag{9}$$

where $L/2\zeta$ is the number of pinned segments of length ζ, with each segment of length ζ finding a local environment that has, on average, the typical binding energy $\sigma_{\Delta U_{\rm tot}}$. We have factored out the length ζ from the potential energy so that the key quantity $\Delta\tilde{E}_p(w)$ appears explicitly. The equilibrium dislocation configuration is then found by minimizing the total energy $\Delta E_{\rm tot}$ with respect to both ζ and w to obtain ζ_c and w_c. Minimization with respect to ζ is analytical, giving

$$\zeta_c(w) \;=\; \left(4\sqrt{3}\frac{\Gamma^2 w^4 b}{\Delta\tilde{E}_p^2(w)}\right)^{\frac{1}{3}}. \tag{10}$$

Minimization of $\Delta E_{\rm tot}$ with respect to w then reduces to the solution of $\partial\Delta\tilde{E}_p(w)/\partial w = \Delta\tilde{E}_p(w)/2w$. $\Delta\tilde{E}_p(w)$ is not explicit in w, and thus minimization is performed numerically. In the theory, w_c emerges naturally via minimizing the total energy.

The above analysis shows that the total energy of the wavy dislocation described by ζ_c and w_c is lower than the original straight dislocation by an energy per unit length of

$$\Delta E_{\rm tot}(\zeta_c, w_c)/L = -\frac{3^{\frac{2}{3}}}{8\cdot 2^{\frac{1}{3}}}\left(\frac{\Delta\tilde{E}_p^4(w_c)}{b^2 w_c^2\Gamma}\right)^{\frac{1}{3}}, \tag{11}$$

where the numerical factor is related to the crystallography of the slip system. This describes the typical pinning of the dislocation by the random field of solutes.

3.4. Thermal activation of dislocation glide

Motion of the overall dislocation then occurs by the motions of the individual segments of length ζ_c. In the pinned configuration, each $2\zeta_c$ portion of the dislocation resides in a local total energy minimum, of average depth $2\zeta_c\Delta E_{\rm tot}(\zeta_c, w_c)/L$ with respect to the zero energy. Along the glide plane, at typical distance w_c away from that minimum, there is a local maximum energy corresponding to an unfavorable solute configuration. We envision this local potential energy landscape to be locally sinusoidal, and the associated potential energy barrier $\Delta E_b'$, *i.e.* the average energy between the local minimum and the local maximum, is then a factor of $\sqrt{2}$ larger than the minimum energy [17]. The total energy barrier ΔE_b to unpin the $2\zeta_c$ dislocation segment must then include a reduction by the elastic energy gain $\Delta E_{\rm LT}$, such that the final energy barrier is given by

$$\Delta E_b \;=\; 1.22\left(\frac{w_c^2\Gamma\Delta\tilde{E}_p^2(w_c)}{b}\right)^{\frac{1}{3}}, \tag{12}$$

with 1.22 emerging as a combination of derived numerical constants.

To glide, the dislocation must overcome ΔE_b by thermal activation. The analysis from this point is standard. An applied resolved shear stress τ facilitates the thermal activation by providing the work $-\tau b\zeta_c x$ on the ζ_c segment as it glides a distance x within the local energy landscape away from the minimum energy position. The local energy landscape in the presence of an applied stress is then

$$E(\tau, x) = \frac{\Delta E_b}{2}\left(1 - \cos\left(\frac{\pi x}{w_c}\right)\right) - \tau b\zeta_c x\,. \tag{13}$$

With increasing τ the effective energy barrier steadily decreases, as shown schematically in Fig. 4. At a sufficiently high stress, the energy barrier becomes zero and the dislocation can glide forward without any thermal activation. This stress is therefore the zero-temperature yield stress τ_{y0}. For the potential energy landscape of Eq. (13), the zero-temperature yield stress is analytically obtained as

$$\tau_{y0} \;=\; \frac{\pi}{2}\frac{\Delta E_b}{b\zeta_c(w_c)w_c} = 1.01\left(\frac{\Delta\tilde{E}_p^4(w_c)}{\Gamma b^5 w_c^5}\right)^{\frac{1}{3}}. \tag{14}$$

At lower stresses $\tau < \tau_{y0}$, the energy barrier is finite. The barrier versus stress, shown schematically in Fig. 4, can be determined from Eq. (13) and for τ near τ_{y0} can be written as [27]

$$\Delta E\,(\tau) = \Delta E_b\left[1 - \left(\frac{\tau}{\tau_{y0}}\right)\right]^{\frac{3}{2}}. \tag{15}$$

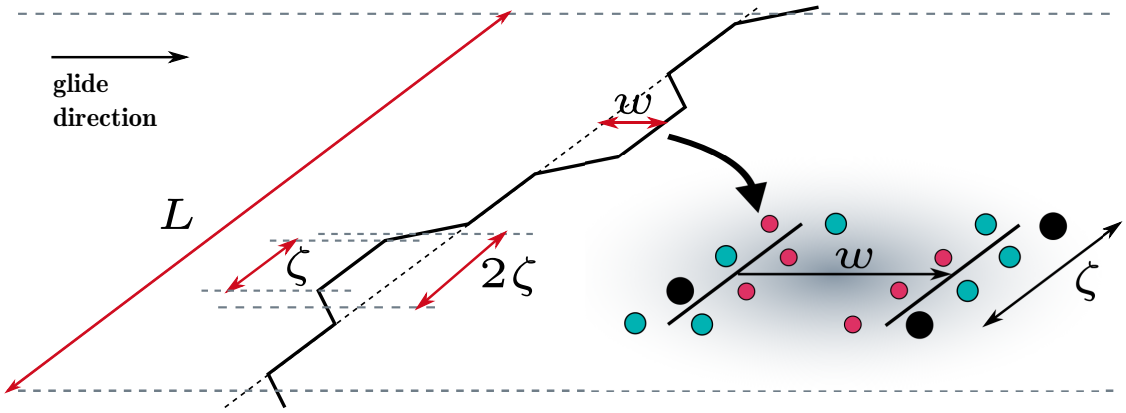

Figure 3: Schematic of the low-energy wavy configuration of the dislocation as it moves through the 3d random field of solutes. The configuration is characterized by segments of lateral length 2ζ of amplitude w along the length of the long dislocation. The key quantity is the change in energy of a straight segment of length ζ as it glides a distance w through the random solute field. The total dislocation energy is minimized with respect to both ζ and w to obtain the controlling characteristic lengths ζ_c and w_c.

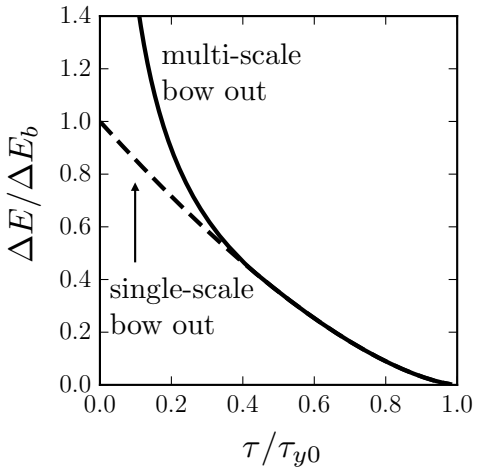

Figure 4: Normalized energy barrier $\Delta E/\Delta E_b$ versus normalized stress τ/τ_{y0}, where ΔE_b and τ_{y0} are the zero-stress energy barrier and zero-temperature flow stress, respectively. Solid line: multiscale bow out model that applies across all stress levels; Dashed line: single-scale bow out model that is accurate at high stresses, and thus controls the strength at low temperatures, as given by Eq. (15).

3.5. Yield Stress versus Temperature and Strain Rate

The overall plastic strain-rate is controlled by the rate of thermally activated glide of the dislocation segments over the stress-dependent energy barrier. Orowan's relation for the strain-rate is $\dot{\varepsilon} = \rho_m b v$ where ρ_m is the mobile dislocation density and v is the velocity [20, 26, 56]. The velocity is determined by the rate of escape R of the segments and the typical glide distance $d \sim w_c$ for each event. The rate of escape is the rate of thermal activation of a segment over the barrier, $R = \nu_0 e^{-\Delta E(\tau)/kT}$ where ν_0 is an attempt frequency that is related to the atomic vibration frequency and the number of atoms along the dislocation line segment, $\nu_0 \sim \nu_{\rm at}/(\zeta_c/b)$. Assembling all of these pieces, the plastic strain-rate is then

$$\dot{\varepsilon} \;=\; \frac{\rho_m b^2 w_c \nu_{\rm at}}{\zeta_c}\; e^{-\frac{\Delta E(\tau)}{kT}} = \dot{\varepsilon}_0\; e^{-\frac{\Delta E(\tau)}{kT}}. \qquad (16)$$

Using typical values for well-annealed metals, $\nu_{\rm at} \sim 10^{13}{\rm s}^{-1}$, and with $w_c \sim 1\,{\rm nm}$ and $\zeta_c \sim 10\,{\rm nm}$ emerging from various analyses below, the reference strain-rate is $\dot{\varepsilon}_0 \sim 10^5{\rm s}^{-1}$. Since $\dot{\varepsilon}_0$ will always appear within a logarithm (see below), values within one order of magnitude of this estimate, e.g. from $10^4{\rm s}^{-1}$ to $10^6{\rm s}^{-1}$, make little quantitative difference in final predictions of the yield strength versus temperature at typical experimental strain rates of $\dot{\varepsilon} = 10^{-5}{\rm s}^{-1}$ to $10^{-2}{\rm s}^{-1}$.

Solving Eq. (16) for the finite-temperature, finite strain-rate yield stress $\tau_y(T,\dot{\varepsilon})$ gives, for $\tau_y/\tau_{y0} \geq 0.5$

$$\tau_y(T,\dot{\varepsilon}) \quad = \quad \tau_{y0}\left[1-\left(\frac{kT}{\Delta E_b}\ln\frac{\dot{\varepsilon}_0}{\dot{\varepsilon}}\right)^{\frac{2}{3}}\right]. \qquad (17)$$

This is a standard formulation in historical solute-strengthening theories (see, for example, Refs. [20, 56]).

With increasing temperature, Labusch [67, 57] argued that the dislocation can become wavy on multiple larger scales, finding ever-deeper energy barriers over longer length scales. He concluded that the relevant energy barrier increases logarithmically with decreasing stress at low stresses, but did not provide a quantitative analysis for evaluation. We have recently derived [68] a related result based upon a generalization of our analysis above for single-scale bow out to multiple-scale bow out. We have demonstrated that there is indeed a transition toward a regime with an approximately logarithmic scaling of the energy barrier versus stress. At even lower stresses, there is a transition to a power-law regime, but this regime tends to be below the regime probed in most available experiments. The energy barrier emerging from the multiscale bow out analysis is shown in Fig. 4 along with the single-scale bow out model. Fitting our full multi-scale bow out analysis to a logarithmic form over an intermediate range of stresses $0.2 \leq \tau_y/\tau_{y0} \leq 0.5$ gives a yield stress versus temperature and strain-rate of [17, 67, 68]

$$\tau_y(T,\dot{\varepsilon}) = \tau_{y0}\exp\left(-\frac{1}{0.57}\frac{kT}{\Delta E_b}\ln\frac{\dot{\varepsilon}_0}{\dot{\varepsilon}}\right), \qquad (18)$$

This logarithmic result can actually be used at stresses up to $\tau_y/\tau_{y0} \approx 0.8$ with very modest errors of approximately 7% over the result of Eq. (17).

For polycrystalline materials, the predicted strength $\tau_y(T,\dot{\varepsilon})$ needs to be converted into an uniaxial yield stress $\sigma_y(T,\dot{\varepsilon})$. For an equiaxed fcc polycrystal, the uniaxial tension strength is obtained from the shear strength by multiplying by the Taylor factor of 3.06.

3.6. Activation Volume

A quantity associated with the finite temperature thermal activation and yield stress is the area swept by the dislocation during the activation process. This area multiplied by the Burgers vector is the activation volume $V = -\partial\Delta E(\tau)/\partial\tau$. For the high-stress/low-temperature model (Eq. (17)), the activation volume can be directly calculated from Eq. (15) as

$$V = \frac{3}{2}\frac{\Delta E_b}{\tau_{y0}}\left(\frac{kT}{\Delta E_b}\ln\frac{\dot{\varepsilon}}{\dot{\varepsilon}}\right)^{\frac{1}{3}}. \qquad (19)$$

Basinksi [44] first experimentally observed that the relationship between the activation volume V and the finite temperature yield stress τ_y seemed independent of the alloy composition for a given temperature. This "stress equivalency principle" is nominally satisfied by the model, provided that the quantity w_c does not vary much between different alloy compositions (which turns out to be the case in the dilute limit for a given matrix material [17, 69]). Then, for a single solute of concentration c, the quantity $\Delta\tilde{E}_p(w_c)^2$ controls both τ_{y0} and ΔE_b, which leads to a direct relationship between V and τ_y. For the high-stress/low-temperature solution, this relationship takes the form $\tau_y = K_1 V^{-3/2}(1 - K_2 V^{1/2})$, where K_1 and K_2 are constants. When $K_2 V^{1/2}$ is small, the relationship between V and τ_y can be approximated by the power law $V \sim \tau_y^{2/3}$, which was previously derived by Nabarro [70].

4. Valuable and Insightful Simplifications

The present theory predicts solute strengthening due to the mesoscale fluctuations on the scale of (ζ_c, w_c) that create the dominant energy barriers controlling thermally-activated dislocation motion. All aspects of the theory are well-defined - there are no fitting or adjustable parameters - and thus the theory should be predictive. The major inputs to the theory are the solute/dislocation interaction energies, which depend on the detailed dislocation structure. The other inputs are the Burgers vector, the elastic constants and the dislocation line tension in the average matrix. The latter is not known precisely, but scales as $\Gamma \propto \mu b^2$ where μ is a representative shear modulus. We will show some specific predictions in Section 5.

However, the full general model does not provide significant direct insights into the role of the average matrix properties, the solute properties, or the overall composition. In addition, the solute/dislocation interaction energies $U^n(x_i, y_j, z_k)$ may not be easily computable or measurable in real materials. Here,

we thus simplify the theory to some important limiting cases: (i) dilute solutions where one component has a high concentration and serves as the "matrix" in which the remaining components are solutes, (ii) elastic interactions only, and (iii) elastic interactions plus a solute/stacking fault interaction model to better account for the dislocation core specific interactions. These simplifications reveal many connections with historical theories, particularly in the dilute limit.

4.1. Dilute limit

To make contact with the historical models, we consider the dilute limit of Eqs. (8), (12) and (14), as most of the efforts in modeling solute strengthening were done for low solute concentration materials.

In this limit, one component n_0 is dominant, *i.e.* $c_{n_0} \gg \{c_{n\neq n_0}\}$, and becomes the matrix element. Each solute n is therefore only surrounded by n_0-type atoms, so the fluctuations of solute/dislocation interactions due to the different possible local chemical and structural environment disappear and the $\sigma_{\Delta U_{ij}^n}$ terms in Eq. (8) vanishes. Applying the sum rule $\sum_n c_n \Delta\overline{U}_{ij}^n(w) = 0$, Eq. (8) can be rewritten as

$$\Delta\tilde{E}_p(w) = \left[\sum_{i,j}\sum_{n\neq n_0} c_n \Delta\overline{U}_{ij}^n(w)^2 + \frac{1}{c_{n_0}}\sum_{i,j}\sum_{\substack{n\neq n_0\\ p\neq n_0}} c_n c_p \Delta\overline{U}_{ij}^n \Delta\overline{U}_{ij}^p\right]^{\frac{1}{2}}. \quad (20)$$

Taking the limit $c_{n\neq n_0} \ll c_{n_0} \simeq 1$, we finally get, neglecting the second order terms in $c_{n\neq n_0}$

$$\Delta\tilde{E}_p(w) = \left[\sum_{i,j}\sum_{n\neq n_0} c_n \Delta\overline{U}_{ij}^n(w)^2\right]^{\frac{1}{2}}. \quad (21)$$

Inserting Eq. (21) into Eqs. (12) and (14), and reducing further to the case of only one solute with concentration c and interaction energy changes $\{\Delta U_{ij}(w_c)\}$ (binary dilute alloy), the scalings of the zero-temperature flow stress and energy barrier with c emerge as

$$\tau_{y0} = 1.01\left(\frac{\left(\sum_{i,j}\Delta U_{ij}(w_c)\right)^2}{\Gamma b^5 w_c^5}\right)^{\frac{1}{3}} c^{\frac{2}{3}},$$
$$\Delta E_b = 1.22\left(\frac{w_c^2\Gamma\sum_{i,j}\Delta U_{ij}(w_c)}{b}\right)^{\frac{1}{3}} c^{\frac{1}{3}}. \quad (22)$$

The scalings with solute concentration $\tau_{y0} \propto c^{2/3}$ and $\Delta E_b \propto c^{1/3}$ are similar to those found in the historical collective pinning models [30, 32, 33, 57]. The present analysis provides quantification, *i.e.* analytic derivation of the prefactors, in terms of the fundamental solute/dislocation interaction energies.

If the solute/dislocation interaction energies and the line tension parameter α are not known, Eqs. (22) can be used to fit experimental measurements with only two parameters over arbitrary temperature and concentration ranges. These parameters are the concentration-normalized energy barrier $\Delta E_b/c^{1/3}$ and zero-temperature flow stress $\tau_{y0}/c^{2/3}$. Examples of such fittings are shown in Fig. 5 for the Cu-Al [44], Cu-Ge, Cu-Mn [51] and Ag-Al [41] systems. The fitted parameters are summarized in Table 1. A similar analysis was performed by Argon [20] and related fitting performed by Toda-Caraballo and Rivera [71], although these fits were unable to capture the high temperature behavior of the yield stress. The latter authors noticed that, for some alloys, a change in energy barrier at a transition temperature was necessary to account for the high temperature behavior in the fitting procedure and this is naturally accomodated within the present theory.

Table 1: Concentration-normalized energy barrier $\Delta E_b/c^{1/3}$ and zero-temperature yield stress $\tau_{y0}/c^{2/3}$ for various dilute binary alloys, as obtained by fitting to experimental data.

	$\Delta E_b/c^{1/3}$ (eV)	$\tau_{y0}/c^{2/3}$ (MPa)
Cu-Al [44]	3.96	187.3
Cu-Ge [51]	3.02	227.2
Cu-Mn [51]	4.01	415.5
Ag-Al [41]	4.30	97.2

Finally, we return to the multiple solute case in the dilute limit. If the minimized w_c for each individual solute value does not vary significantly across the range of solutes considered (verified for solutes

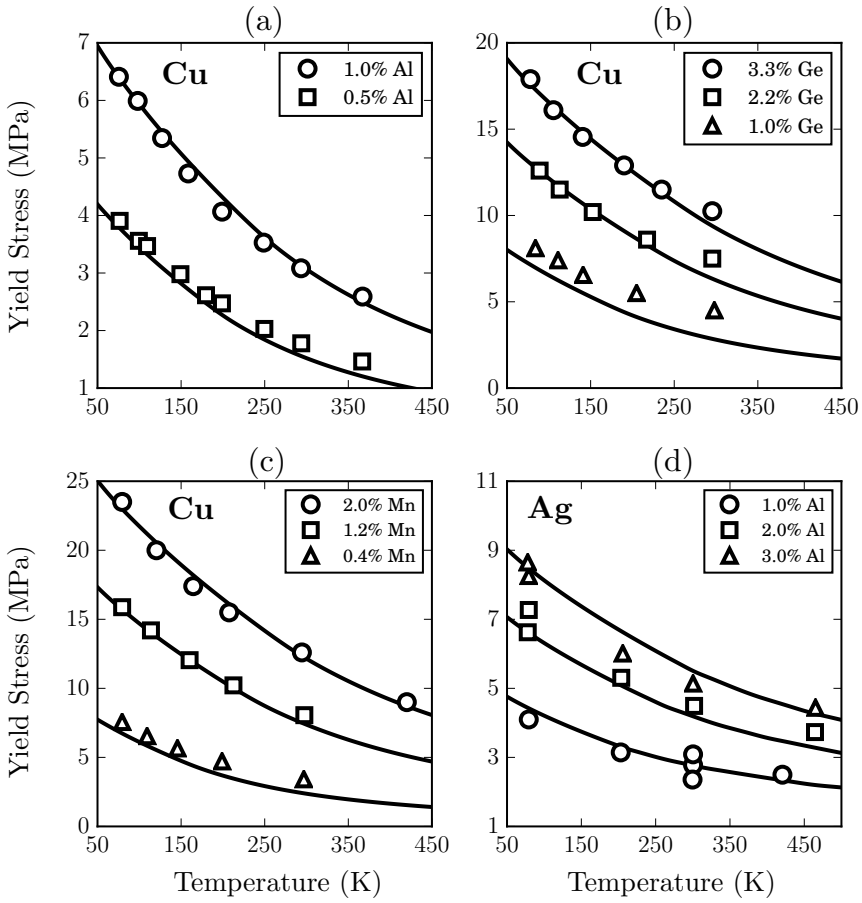

Figure 5: Yield stress versus temperature, as predicted by multiscale bow out model (lines) and as measured (symbols): (a) Cu-Al [44]; (b) Cu-Ge [51], (c) Cu-Mn [51] and (d) Ag-Al [41]. Predictions use fitted parameters in Table 1.

in Al by Leyson *et al.* [17]), then the approximate relationship

$$\tau_{y0} = \left[\sum_n \left(\tau_{y0}^{(n)}\right)^{\frac{3}{2}}\right]^{\frac{2}{3}}, \Delta E_b = \left[\sum_n \left(\Delta E_b^{(n)}\right)^3\right]^{\frac{1}{3}}, \tag{23}$$

holds where $\tau_{y0}^{(n)}$ and $\Delta E_b^{(n)}$ are the zero-temperature flow stress and energy barrier for solute n alone. The first expression in Eq. (23) is consistent with Labusch's analysis [32, 33], which implicitly assumed some constant value of the w cut-off parameter.

4.2. Elastic interaction model

We now simplify the full strengthening theory of Eqs. (8), (12) and (14) by considering only the elasticity contribution $U_{\rm el}^n(x_i, y_j, z_k) = -p(x_i, y_j)\Delta V_n(x_i, y_j, z_k)$ to the solute/dislocation interaction energy, which is due to the interaction between the pressure field $p(x_i, y_j)$ of the dislocation at the solute site and the solute n misfit volume at this site. This "size" contribution is common to all materials. Furthermore, in substitutional fcc materials, due to cubic symmetry, the effects of local deviatoric misfit strains of solutes average to zero. The elasticity limit also enables comparison with simpler literature models based on elasticity concepts.

We first express the dislocation pressure field as $p(x_i, y_j) = -\frac{\mu}{3\pi}\frac{(1+\nu)}{(1-\nu)}f(x_i, y_j)$ where $f(x_i, y_j)$ is the dimensionless pressure generated by the distribution of normalized Burgers vector along the glide plane (see for instance Fig. 2c). Here, μ is the isotropic shear modulus so that anistropic elastic

effects are embedded within the function f. Inserting the above into Eq. (8), the key energy in the theory becomes

$$\Delta\tilde{E}_p(w) = \frac{\mu}{3\pi}\frac{(1+\nu)}{(1-\nu)}\left[\sum_{i,j}\Delta f_{ij}^2(w)\right]^{\frac{1}{2}} \times \left[\sum_n c_n\left(\Delta\overline{V}_n^2+\sigma_{\Delta V_n}^2\right)\right]^{\frac{1}{2}}, \quad (24)$$

where $\Delta f_{ij}(w) = f(x_i - w, y_j) - f(x_i, y_j)$. Recall that $\Delta\overline{V}_n$ is the average misfit volume of solute n and $\sigma_{\Delta V_n}$ its standard deviation due to different local chemical and structural environments.

Minimization of the total energy with respect to w to determine w_c is then determined only by $\Delta f_{ij}(w)$; the role of the dislocation core structure is thus separated from the solute properties. In other words, w_c depends *only* on the dislocation core structure through the dislocation pressure field. After minimization, we obtain (ζ_c, w_c) for the specific dislocation core structure. Without any loss of generality, we can express the line tension for bowing in the glide plane as $\Gamma = \alpha\mu b^2$, with α a dimensionless number that may also incorporate anisotropic elasticity. The zero-temperature flow stress τ_{y0} and energy barrier ΔE_b can then be written as

$$\tau_{y0} = 0.051\ \alpha^{-\frac{1}{3}}\mu\left(\frac{1+\nu}{1-\nu}\right)^{\frac{4}{3}} f_1(w_c) \times \left[\frac{\sum_n c_n\left(\Delta\overline{V}_n^2+\sigma_{\Delta V_n}^2\right)}{b^6}\right]^{\frac{2}{3}}, \quad (25)$$

$$\Delta E_b = 0.274\ \alpha^{\frac{1}{3}}\mu b^3\left(\frac{1+\nu}{1-\nu}\right)^{\frac{2}{3}} f_2(w_c) \times \left[\frac{\sum_n c_n\left(\Delta\overline{V}_n^2+\sigma_{\Delta V_n}^2\right)}{b^6}\right]^{\frac{1}{3}}, \quad (26)$$

where $f_1(w_c) = \left[\left(\frac{b}{w_c}\right)^{5/2}\sum_{i,j}\Delta f_{ij}^2(w_c)\right]^{2/3}$ and $f_2(w_c) = \left[\left(\frac{w_c}{b}\right)^{2}\sum_{i,j}\Delta f_{ij}^2(w_c)\right]^{1/3}$ are the *minimized* coefficients for the given core structure.

Two interesting features emerge when examining the role of the core structure for dislocations that dissociate into two partial dislocations separated by a stacking fault of length d, as in fcc crystals, and basal and pyramidal slip in hcp crystals. We first represent the core structure by a distribution of Burgers vector along the glide plane, and compute the pressure using isotropic linear elasticity (see Appendix A and Fig. A.13 for details). Then, for sufficiently large d, the minimization to obtain w_c and the coefficients $f_1(w_c)$ and $f_2(w_c)$ reveals the existence of two minima with two values $w_{c,\mathrm{LT}} < d$ and $w_{c,\mathrm{HT}} \approx d$ and thus two sets of coefficients $f_{1,\mathrm{LT}}(w_{c,\mathrm{LT}}), f_{2,\mathrm{LT}}(w_{c,\mathrm{LT}})$ and $f_{1,\mathrm{HT}}(w_{c,\mathrm{HT}}), f_{2,\mathrm{HT}}(w_{c,\mathrm{HT}})$. The first minimum has a higher strength $f_{1,\mathrm{LT}}(w_{c,\mathrm{LT}}) > f_{1,\mathrm{HT}}(w_{c,\mathrm{HT}})$ but lower energy barrier $f_{2,\mathrm{LT}}(w_{c,\mathrm{LT}}) < f_{2,\mathrm{HT}}(w_{c,\mathrm{HT}})$. The first minimum thus controls the strength at lower temperatures while the second minimum controls the strength at higher temperatures, with low and high depending on the precise material values. The second minimum thus provides a "high temperature plateau" strength that may supplant the high temperature behavior due to the first minimum. This unexpected outcome will appear in our predictions below for Mg-Zn.

Of perhaps more importance is that the coefficients $f_{1,\mathrm{LT}}(w_{c,\mathrm{LT}})$ and $f_{2,\mathrm{LT}}(w_{c,\mathrm{LT}})$ for the first, low temperature, minimum are essentially independent of d for $d > 10b$. For matrices (pure or alloy) with low stacking fault energies γ_{SF}, and thus large d, the low temperature flow stress is therefore independent of stacking fault energy. The coefficients depend on the spreading of the Burgers vectors of the partial dislocations, but these do not vary significantly across fcc metals. This unexpected outcome will enable predictions of flow strength for a range of fcc High Entropy Alloys for which the stacking fault energies are sufficiently low (such that $d > 10b$) but are not established with any quantitative accuracy.

With coefficients $f_{1,\mathrm{LT}}(w_{c,\mathrm{LT}})$ and $f_{2,\mathrm{LT}}(w_{c,\mathrm{LT}})$ independent of material (for $d > 10b$), the above elastic theory becomes fully analytical. Eqs. (25) and (26) then show that high strength materials are achieved by maximizing the shear elastic modulus of the matrix (which itself encourages larger $d = \mu b(2+\nu)/(24\pi(1-\nu)\gamma_{\mathrm{SF}})$ for fcc edge dislocations) and maximizing the concentration-weighted mean-squared misfit volume quantity. The importance of high shear elastic modulus and high misfit parameter appear in previous models for dilute alloys [29, 32, 39, 69], but the result here is now generalized for arbitrary composition of the solid solution alloys and is demonstrated to be independent of dislocation dissociation for $d > 10b$.

Furthermore, the concentration-weighted mean-

squared solute misfit volume quantity appearing in Eqs. (25) and (26) can be related - under certain conditions - to the so-called "lattice misfit parameter" δ. Specifically, neglecting the fluctuations in solute/dislocation interactions, assuming that all alloying elements can crystallize in the same structure, and assuming that Vegard's law is followed for the lattice parameter variations with alloy composition, the misfit parameter is $\delta = \sqrt{\sum_n c_n \Delta\overline{V}_n^2}/3\overline{V}$, with $\overline{V}$ the atomic volume of the average matrix. The zero-T strength and energy barrier thus scale as $\tau_{y0} \propto \delta^{4/3}$ and $\Delta E_b \propto \delta^{2/3}$. This δ parameter is frequently estimated [6, 72, 73, 74] using tables of "accepted" atomic radii for the different elements. Such estimates are generally not sufficiently accurate for real predictions and should be replaced by the more general definition using the misfit volumes of the solutes in the actual alloy of interest. These misfit volumes are well-defined quantities from both thermodynamics and mechanics perspectives, do not rely on any Vegard's law assumption, do not require the elements to crystallize in the same structure, and are simple enough to be computable using *ab initio* calculations [13, 17, 75].

Reducing again to the case of only one dilute solute with concentration c and misfit volume ΔV, we obtain the zero-temperature flow stress and energy barrier for dilute binary alloys as

$$\begin{aligned} \tau_{y0} &= 0.051\alpha^{-\frac{1}{3}}\mu\left(\frac{1+\nu}{1-\nu}\right)^{\frac{4}{3}} f_1(w_c)\; c^{\frac{2}{3}}\; \frac{\Delta V^{\frac{4}{3}}}{b^4}, \\ \Delta E_b &= 0.274\alpha^{\frac{1}{3}}\mu b^3\left(\frac{1+\nu}{1-\nu}\right)^{\frac{2}{3}} f_2(w_c)\; c^{\frac{1}{3}}\frac{\Delta V^{\frac{2}{3}}}{b^3}. \end{aligned} \tag{27}$$

These scalings with the solute misfit volume, $\tau_{y0} \propto \Delta V^{4/3}$ and $\Delta E_b \propto \Delta V^{2/3}$ [17, 69], show that ΔV is a sensitive quantity for which an accurate determination is necessary. However, ΔV can now be achieved by routine *ab initio* computations. Note that the sign of the misfit volume does not have any importance within the simplified model adopted here, *i.e.* solutes having misfit volumes of the same magnitude but with opposite signs will strengthen the material in the same way. This is revealed in explicit calculations for Mg and Cu solutes in fcc Al, for instance [17].

If the solute(s) modify the elastic constants of the average matrix relative to the pure elemental matrix then, in the dilute binary alloy case, we can write $\mu = \mu_0 + (\partial\mu/\partial c)c$, giving rise to a second-order dependence on concentration c in both τ_{y0} and ΔE_b. This provides one component of the historical "modulus" term in the strengthening. As summarized by Argon [20], the change in elastic constants induced by the presence of solutes in a pure element has two main consequences: (i) additional core-specific interactions (inhomogeneity or "modulus" Fleischer effect [20, 28, 29]) and (ii) modification of the dislocation line tension. The simplified model based on misfit interactions in the average matrix does not include the first effect, but does create a concentration-dependence of the dislocation pressure field and the line tension. In the full model, Eqs. (8), (12) and (14), core interactions are computed atomistically by DFT, meaning that the "modulus" effect and all other higher order effects occurring within the dislocation core are automatically included (cf. description of solute/dislocation interactions in section 2).

4.3. Additional core contribution: interaction with the stacking fault

As mentioned above, the reduced elasticity misfit volume interaction model for the solute/dislocation interaction neglects all specific chemical interactions within the dislocation core. In fcc materials, dislocations are dissociated into two partials separated by a stacking fault. An alternative to direct calculations that improves the interaction description within the core zone without adding too much complexity is to consider also the interaction of the solute with the stacking fault in this region. This has been done in the work of Yasi *et al.* [39] and Ma *et al.* [76] for dilute binary alloys, in the framework of a Fleischer-type and Leyson-type strengthening model, respectively. This led to the identification of important features due to the specific core interactions, as will be seen further below. We discuss here the dilute binary case for simplicity. The total interaction energy for the solute n at a given position (x_i, y_j) becomes the sum of the misfit term and a stacking fault term

$$U^n(x_i, y_j) = -p(x_i, y_j)\Delta\overline{V}_n + U^n_\gamma(x_i, y_j), \tag{28}$$

The stacking fault term $U^n_\gamma(x_i, y_j)$ can be approximated as constant within the stacking fault and zero outside, so that

$$U^n_\gamma(x_i, y_j) = U^n_{\gamma_1}\delta_{j\pm1}\left[H\left(x_i + \frac{d}{2}\right) - H\left(x_i - \frac{d}{2}\right)\right], \tag{29}$$

where $\delta_{j\pm1}$ is the Kronecker symbol, $d \leq d_{\rm eq}$ the equilibrium dislocation dissociation distance and H the Heaviside function, which delineates the range along the glide plane where the interaction with the stacking fault exists. This accounts for the interaction energy $U^n_{\gamma_1}$ of the solute with the stacking fault over the two planes adjacent to the glide plane that define the stacking fault plane. Note that interactions of substitutional solutes in planes farther away from the stacking fault can exists [37] and can be included in Eq. (29) by considering $j = \pm 2, 3, ...$ Interstitial solutes and/or multiple solute sites not related by symmetry [77, 78] are also straightforward to consider. However, in such cases, and even when considering only the two planes adjacent to the stacking fault energy, the Heavyside function may require some smoothing to avoid an abrupt transition in the energy contributions versus distance w. This does not change the general conclusions below. The solute/stacking fault interactions can be calculated using direct *ab initio* calculations, now routinely done for dilute alloys [77, 78, 79, 80].

Using the interaction model of Eq. (28), the key characteristic energy $\Delta\tilde{E}_p(w)$ becomes

$$\Delta\tilde{E}_p(w) = \Bigg[\Delta\overline{V}_n^2 \sum_{i,j} \Delta p_{ij}^2(w) + {U^n_{\gamma_1}}^2 \sum_{i,j} \Delta h_{ij}^2(w) - 2\Delta\overline{V}_n U^n_{\gamma_1} \sum_{i,j} \Delta p_{ij}(w) \Delta h_{ij}(w) \Bigg]^{\frac{1}{2}} c^{\frac{1}{2}}. \quad (30)$$

with

$$\Delta p_{ij}(w) = -\frac{\mu}{3\pi}\frac{(1+\nu)}{(1-\nu)}\Delta f_{ij}(w), \quad (31)$$

$$\Delta h_{ij}(w) = \delta_{j\pm1}\left[H\Big(x_i - w + \frac{d}{2}\Big) - H\Big(x_i + \frac{d}{2}\Big) - H\Big(x_i - w - \frac{d}{2}\Big) + H\Big(x_i - \frac{d}{2}\Big)\right]. \quad (32)$$

The key energy $\Delta\tilde{E}_p(w)$ of Eq. (30) can therefore be decomposed into a misfit volume ("size") term, a stacking-fault interaction term, and a cross-term between misfit volume and stacking fault interaction. Interestingly, contrary to the case of the misfit volume interaction only, the role of the solute and matrix properties are no longer separated. The minimization with respect to w leading to w_c is not independent of the solute properties. Ma *et al.* [76] illustrated this aspect by showing a dependence of w_c on misfit volume and stacking fault interaction energies when both terms are included for the solute/dislocation interactions.

Both zero-temperature flow stress and energy barrier scale with the key energy $\Delta\tilde{E}_p(w_c)$, *i.e.* we have $\tau_{y0} \propto \Delta\tilde{E}_p(w_c)^{4/3}$ and $\Delta E_b \propto \Delta\tilde{E}_p(w_c)^{2/3}$. Consequently, the first two terms in Eq. (30) are always positive and increase the strength at any temperature, whatever the sign of $\Delta\overline{V}_n$ and of U^n_γ. However, their respective signs matter for the third term (the cross-term), which can either enhance or decrease the strength. Similar conclusions were obtained using approximate functional forms for the zero-temperature strength by Yasi *et al.* [39] and for both zero-temperature strength and energy barrier by Ma *et al.* [76]. Note that these authors adopt a slightly different expression for the interaction of the solute between the two partials, considering a slip misfit parameter

$$\epsilon_{\rm SF} = \frac{1}{\gamma_{\rm SF}}\frac{d\gamma_{\rm SF}}{dc}\bigg|_{c=0}, \quad (33)$$

with $\gamma_{\rm SF}$ the relevant stable stacking fault energy of the material. The solute/dislocation interaction is then given by

$$U^n_\gamma(x_i, y_{\pm1}) = A_s\gamma_h\left(\mathbf{u}_s(x_i, y_{\pm1})\right)\epsilon_{\rm SF}, \quad (34)$$

where A_s is the area of the solute atom projected on the slip plane, γ_h is the generalized stacking fault energy of the host, $\mathbf{u}_s$ is the shear displacement of the atom adjacent to the stacking fault with coordinates $(x_i, y_{\pm1})$. This formulation should better describe the interaction of the solutes when approaching the partial cores than the simple model of Eq. (29), as it accounts for the exact misfitting displacement along glide direction instead of having an abrupt Heaviside function. On the other hand, inclusion of the interaction of solutes located in planes farther away from the glide plane is less obvious within this approach and would require additional modeling [77, 80].

To conclude, simplified models to account for both elastic long-range effects and chemical-specific short-range interactions within the dislocation core allows us to tackle and understand the possible consequences of including core interactions, compared to the purely elastic case: (i) variation of w_c with the solute type (seen in Al alloys [17], although changes are very weak), and (ii) strengthening/softening compared to the simplified misfit volume interaction model. Finally, the elas-

tic/stacking fault interaction models require material input that are obtained from comparatively low-cost *ab initio* simulations, thus allowing for the construction of design maps at a low cost, as compared to full direct computations of the solute/dislocation interactions (see examples by Yasi *et al.* [39] for Mg alloys and Ma *et al.* [76] for Al alloys).

5. Applications

We now turn to various applications of the strengthening model to materials having low intrinsic Peierls stress. We select specific cases here that are not addressed in detail in earlier work, so that the results here are new in some respects. The applications cover a range of systems, one with a relatively compact dislocation core (fcc Al alloys), one with well-dissociated and distinct partial dislocations (basal slip in hcp Mg alloys), one with the dislocation at an interface (twinning in Mg), and finally complex non-dilute alloys (fcc High Entropy Alloys). Each application demonstrates the quantitative, parameter-free power of the theory while also revealing new predictions that emerge naturally from the theory.

5.1. Al-Mn Solid Solutions

We have previously examined the strengthening behavior of various solutes in Al alloys [17, 69]. Here, we specifically discuss the case for Mn solutes in fcc Al, and pay detailed attention to the role of the line tension. The edge dislocation core was computed by previously [81] and corresponds to the structure shown in Fig. 1a. Based on this structure, the normalized pressure field of the dislocation away from the core is described using the following spread core model,

$$f(x_i,y_j)=\frac{b}{n+1}\sum_{l=-\frac{n}{2}}^{\frac{n}{2}}\frac{y_j}{\left[x_i-l\left(\frac{b}{2}\right)\right]^2+y_j^2}, \qquad (35)$$

where $n=10$, which was previously shown to agree well with the core predicted using an EAM potential [82]. A Peierls-Nabarro model [26] could also be used, or a double-Gaussian model as shown in Fig. 2c. The solute/dislocation interaction outside the dislocation core is assumed to be purely elastic, *i.e.* $U_{\rm el}(x_i,y_j)=-p(x_i,y_j)\Delta V$. For sites immediately adjacent to the dislocation core (stacking fault region), the interaction energy is calculated by direct substitution of an Al atom by a Mn atom in the quantum computational cell. The resulting map of solute/dislocation interaction energy versus solute position is shown in Fig. 1a. This is the only solute input to the theory.

The line tension Γ is a material property, but its precise value is not well-established since it involves dislocation core energies. In addition, since line tension is in part controlled by elastic interactions along a non-straight dislocation, the line tension varies with the length of the bowing line. In the context of solute strengthening, the line tension should thus be computed at the characteristic periodic length $2\zeta_c$. Recent atomistic calculations for Al using an EAM potential [83] showed that Γ for the edge dislocation is approximately

$$\Gamma=C_1\ln(2\zeta_c/b)+C_0, \qquad (36)$$

where $C_1=0.072$ eV.Å^{-1} and $C_0=-0.04$ eV.Å^{-1}. The theory above assumed that the line tension is independent of ζ and so is not included in minimization of the total energy. Since the line tension only varies logarithmically with ζ_c, the additional complexity has minor quantitative effects. For instance, for Mn concentrations ranging from 0.001–0.01, ζ_c varies in the range 150–300 Å, and Eq. (36) then predicts Γ to range from 0.30–0.35 eV.Å^{-1}. The zero temperature strength and energy barrier scale weakly with Γ, as $\tau_{y0}\sim\Gamma^{-1/3}$ and $\Delta E_b\sim\Gamma^{1/3}$ respectively, so that effects of such variations in line tension are minor. The values 0.30–0.35 eV are slightly lower, however, than the value of 0.47 eV.Å^{-1} used in Ref. [17]. The line tension Γ could also be calculated self-consistently using the model and the relationship between Γ and ζ_c given in Eq. (36). Specifically, an initial value for Γ is assumed and is used to calculate ζ_c. A new line tension $\Gamma'(\zeta_c)$ is then computed and used to predict a new value of $\zeta_c'\sim\Gamma'^{-1/3}$. This process is iterated until both ζ_c and Γ are converged. The resulting self-consistent Γ then determines the solute strengthening parameters $\Delta E_b\sim\Gamma^{-1/3}$ and $\tau_{y0}\sim\Gamma^{1/3}$.

The total energy vs. w for Al-Mn is shown in Figure 6a. For the Al core with small partial dislocation separation, only a single minimum emerges at a characteristic length $w_c=18.6$Å that is on the order of the partial separation. The resulting solute strengthening parameters for Al-Mn are summarized in Table 2. For comparison, the same parameters as predicted by Ma *et al.* [76] using the

Table 2: Solute strengthening parameters for the Al-Mn and Mg-Zn systems. The Mg-Zn system has two sets of parameters, corresponding to each minimum shown in Fig. 6. The parameters shown use $\Gamma = 0.32$ eV/Å and $\Gamma = 0.24$ eV/Å for Al-Mn and Mg-Zn, respectively. Values between parenthesis are from Ref. [76].

Normalized parameter	Al-Mn	Mg-Zn	
		Conf 1	Conf 2
w_c (Å)	18.6(17.1)	9.6	35.1
$\zeta_c \cdot c^{\frac{1}{3}}$ (Å)	38.8	31.8	108.4
$\Delta E_b / c^{\frac{1}{3}}$ (eV)	6.62(6.94)	1.61	5.76
$\tau_{y0} / c^{\frac{2}{3}}$ (MPa)	807.9(840)	416.5	108.9

same strengthening theory but a simplified elastic/stacking fault interaction model (see Eqs. 29 and 34) are also shown; similar values are found, showing the validity of the simplified interaction model for Al-Mn alloys. The predictions of the model are compared to experimental measurements by Diak *et al.* [49] on three different alloy compositions at temperatures ranging from 78K to 263K and $\dot{\varepsilon} = 5 \times 10^{-5}\text{s}^{-1}$. The theory uses a reference strain-rate of $\dot{\varepsilon}_0 = 10^4\text{s}^{-1}$. Diak *et al.* have confirmed that their alloys contained elements other than Mn, but only in negligible concentrations. In particular, Fe concentrations are less than 3 ppm; this is especially important because solute strengthening of Fe in Al is anomalously large [17, 69]. Moreover, the present theory fails in prediction of the strength of dilute Al-Fe binary alloys; this will be discussed in Section 6. The comparison between predictions and experiments for Al-Mn alloys is shown in Fig. 7. For the purpose of illustration, predicted strengths over a range of line tension values are shown to indicate sensitivity of the results to this quantity. A good agreement over the entire concentration and temperature range of the experiments is found. We emphasize here that our predictions are based on first-principles calculations and are parameter-free.

5.2. Activation volume of Al alloys

The activation volume V is a physical quantity that can be measured experimentally using strain jump tests, and Basinski showed that V satisfies the stress-equivalency principle in solute strengthened materials. It was shown earlier that stress equivalency is predicted by the model if w_c is the same for all the alloys, which is well-satisfied in Al-X alloys, and assuming that Γ is a constant. While the finite-temperature yield stress τ_y is only weakly dependent on Γ due to the opposing trends on τ_{y0} and ΔE_b, the activation volume scales like $\Gamma^{5/9}$. It is thus not clear if stress equivalency is obeyed if Γ varies with ζ_c and, therefore, solute concentration. To investigate this issue, we have computed the line tension Γ self-consistently using the model and the relationship between Γ and ζ_c given in Eq. (36), as discussed in the previous paragraph.

We perform the analysis for Al-Mg and Al-Si alloys using solute strengthening parameters reported in Ref. [17], but rescaled with the self-consistent Γ. These alloys are chosen because they have very different ΔE_b and τ_{y0} but the same w_c. The predicted activation volume as a function of τ_y is shown in Fig. 8a in a log-log plot along with the experimental values of Diak *et al.* Diak *et al.* [52, 53] measured at 78 K for a range of solutes in Al. The results show that stress equivalency is upheld even when Γ varies with solute concentration (through the corresponding value of ζ_c). Both the predictions and the experiments in Fig. 8a are approximately linear, indicating a power-law relationship $V \sim \tau_y^{-m}$. The exponent m using the self-consistent Γ is slightly larger than that using a fixed Γ but both cases are smaller than experiments. The predicted magnitude of V is larger than experiments, but the experimental yield stress includes contributions due to lattice friction (Peierls stress) on the order of 1 MPa. When this is taken into consideration, agreement is improved. Finally, an interesting consequence of this analysis is that the variation of Γ with τ_y also shows a "stress equivalency". That is, given the same finite-temperature yield stress, two alloys with the same matrix will have the same characteristic length regardless of the alloying element(s) (the Γ vs. τ_y curve is given in Fig. 8b).

5.3. Mg-Zn Solid Solutions

Unlike the relatively compact dislocation core in Al, the basal edge dislocation in Mg has a large dissociated core with distinct partials, commensurate with its low stacking fault energy. The fundamental theory applies in general, but reveals that a second minimum solution arises in Mg that is absent in Al, and this has implications for the strength at higher temperatures. We first reported on this feature of the model in Ref. [18] for Mg-Al alloys. Here, we present previously unpublished predictions for the Mg-Zn system.

The solute/dislocation interaction energies were calculated by DFT for atomic sites in the Mg basal edge dislocation core by Yasi *et al.* [39], and are

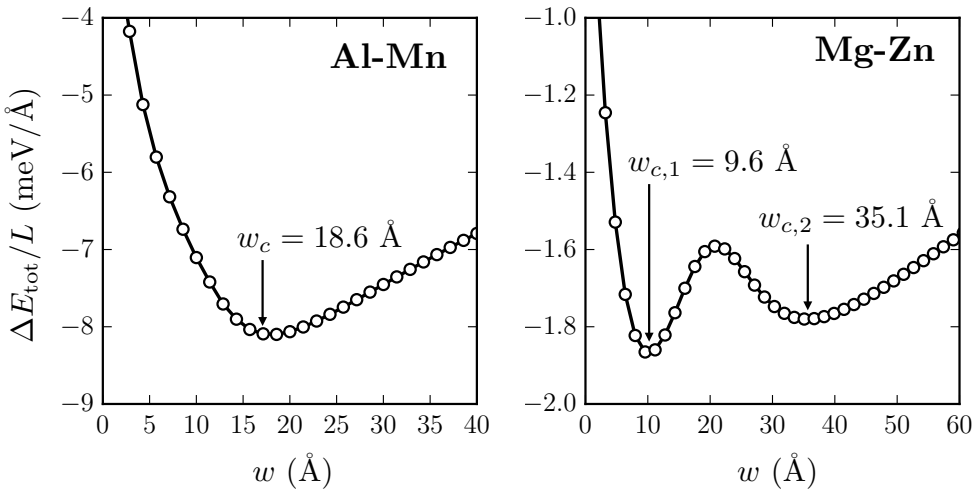

Figure 6: The total energy change per unit length $\Delta E_{tot}/L$ versus distance w. Left plot: Al-Mn, showing a single minimum at $w_c = 18.6$ Å; right plot: Mg-Zn, showing two minima at $w_{c,1} = 9.6$ Å and $w_{c,2} = 35.1$ Å.

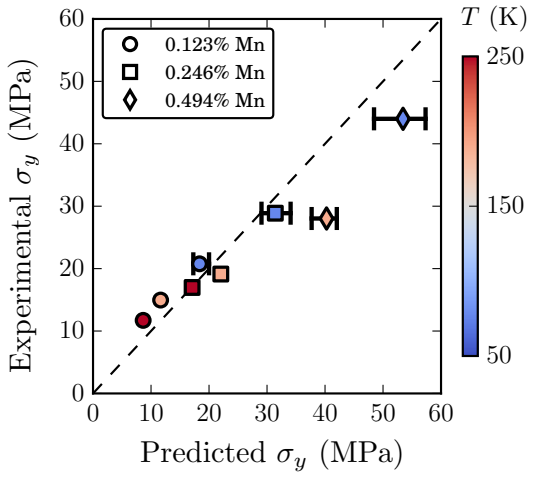

Figure 7: Experimental [52] and predicted finite-temperature yield stress $\sigma_y(T) = 3.06\tau_y(T)$ for Al-Mn alloys. The predicted results use self-consistent line tension Γ values. The range of predicted values corresponds to an assumed range of $\Gamma = 0.2$ to $0.47\,\mathrm{eV.\AA^{-1}}$ to show sensitivity to this parameter; symbols without a range indicate that the range is smaller than the symbol size. The dashed line of slope of unity is a guide to the eye.

shown in Fig. 1b. The solute/dislocation energies outside the core region were approximated by elasticity with the DFT-computed misfit volume $\Delta V = -10.6$ Å^3 for Zn in Mg. For an accurate description of the normalized pressure field $f(x_i, y_j)$, we use the Peierls-Nabarro model,

$$f(x_i, y_j) = \int_{-\infty}^{\infty} \frac{b'(x')\ y_j}{(x_i - x')^2 + y_j^2} dx' \qquad (37)$$

where the Burgers vector distribution $b'(x') = db/dx$ is calculated from the first-principles-computed core structure of Yasi *et al.* [39]. The complete solute/dislocation interaction energy map is shown in Fig. 1b. The smooth transition between the DFT computed core interactions and the elastic misfit volume interactions outside the core region is again found and supports the use of the elasticity approximation just outside the core. We use a line tension based on Eq. (36), but scaled the results from Al to account for the differences in shear modulus and Burgers vector, as $\Gamma = \alpha\mu b^2$. The self-consistent procedure leads to a Γ that ranges from 0.19–0.28 eV.Å^{-1} for the temperature and concentration range in the experiments.

The total energy per unit length as a function of w (see Eq. (11)) for the wavy dislocation is shown in Fig. 6b. Here, the change in total energy shows two minima rather than just one; this was noted earlier during our discussion of the elasticity limit of the general theory. In Mg basal slip, there are therefore

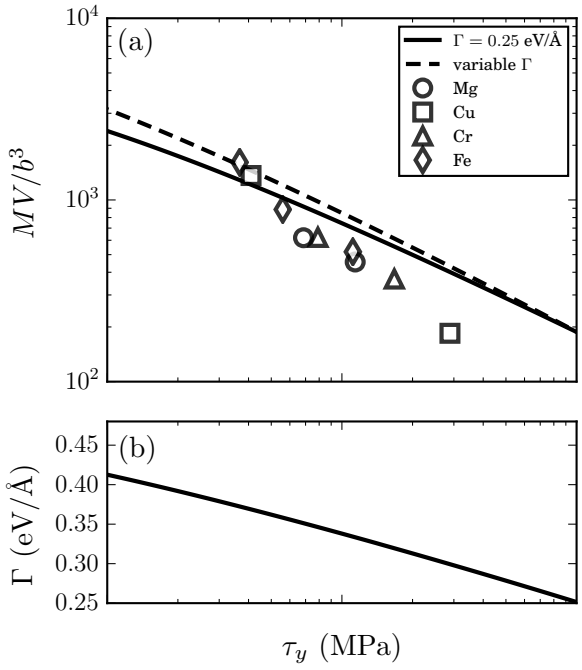

Figure 8: (a) Normalized activation volume MV/b^3 and versus yield stress τ_y at 78 K for experimental binary Al alloys [52, 53] (open symbols) and predictions (solid line: $\Gamma = 0.25$ eV/Å; dashed line: self-consistent Γ). Predictions are calculated using solute strengthening parameters for Al-Mg and Al-Si from Ref. [17], and the results are identical thus demonstrating Basinksi's stress equivalency principle. (b) Self-consistent line tension Γ vs τ_y.

two equilibrium configurations that the dislocation can adopt, leading to two sets of solute strengthening parameters as summarized in Table 2. The two minima arise because of the dissociated nature of the Mg basal edge dislocation core. The first configuration corresponds to a decorrelation of solute fluctuations when the dislocation has moved approximately one-half the partial separation. This configuration is characterized by a relatively large zero-temperature yield stress but a relatively low energy barrier. The second configuration corresponds to decorrelating much longer-range solute fluctuations, and is characterized by a relatively small zero-temperature yield stress but a relatively high energy barrier.

In order to glide, the dislocation must overcome both types of configurations by thermal activation. In general, one of the configurations will dominate, *i.e.* have the largest barrier at any given stress. To determine the net rate of flow, Eq. (16) should thus be replaced by

$$\begin{aligned}\frac{1}{\dot{\epsilon}} =& \frac{1}{\dot{\epsilon_1}} + \frac{1}{\dot{\epsilon_2}} \\ =& \frac{1}{\dot{\epsilon}_\circ}\left[\exp\left(\frac{\Delta E_1(\tau)}{kT}\right) + \exp\left(\frac{\Delta E_2(\tau)}{kT}\right)\right], \quad (38)\end{aligned}$$

where the subscripts 1 and 2 indicate the first and second configurations, respectively. Inverting Eq. (38) yields the prediction of the finite temperature yield stress $\tau_y(T, \dot{\varepsilon})$. Due to the two different configurations, the temperature dependence of the yield stress exhibits two regimes. At low temperatures, since $\Delta E_1 < \Delta E_2$ which leads to $\dot{\varepsilon}_2 \ll \dot{\varepsilon}_1$, the low temperature behavior of Mg basal slip is controlled by the first configuration. At higher temperatures, the second configuration dominates the flow. The transition between the two regimes occurs over a relatively narrow temperature range because the energy barrier appears in an exponential Arrhenius law. The solution to Eq. (38) can be well approximated by using Eqs. (17) and (18) for both configurations and selecting the larger stress.

We now compare the predictions against experiments by Akhtar and Teghtsoonian [84]. They measured the yield stresses of Mg-Zn alloys at concentrations ranging from 0.15% to 0.45% and at various temperatures, at $\dot{\varepsilon} = 1.66 \times 10^{-4}$ s^{-1}. As before, we use $\dot{\varepsilon}_0 = 10^4$ s^{-1}. Because the alloy strengths are comparable to the measured Peierls stress $\tau_y^{\mathrm{Mg,P}}$ of pure Mg , we add $\tau_y^{\mathrm{Mg,P}}$ to the predictions. The yield strength versus temperatures, as predicted and measured, are shown in Fig. 9. With no adjustable parameters or fitting, the predictions are in good agreement with experiments over all concentrations and temperatures. There is some overestimation of the yield stress at low temperatures, but of more importance is that the model nicely captures the transition in strength with increasing temperature into what is traditionally referred to as a "plateau" regime. The presence of a plateau has previously been attributed to additional strengthening mechanisms, such as solute multiplets [51], elastic dislocation/dislocation interactions [85], or solute drag "friction" [20]. Here, the "plateau" regime arises naturally from the theory as a consequence of the well-dissociated nature of the basal dislocations in Mg, and quantitatively explains the trends in experimental results versus temperature and composition. No new or unusual mechanisms need to be invoked to explain the experiments.

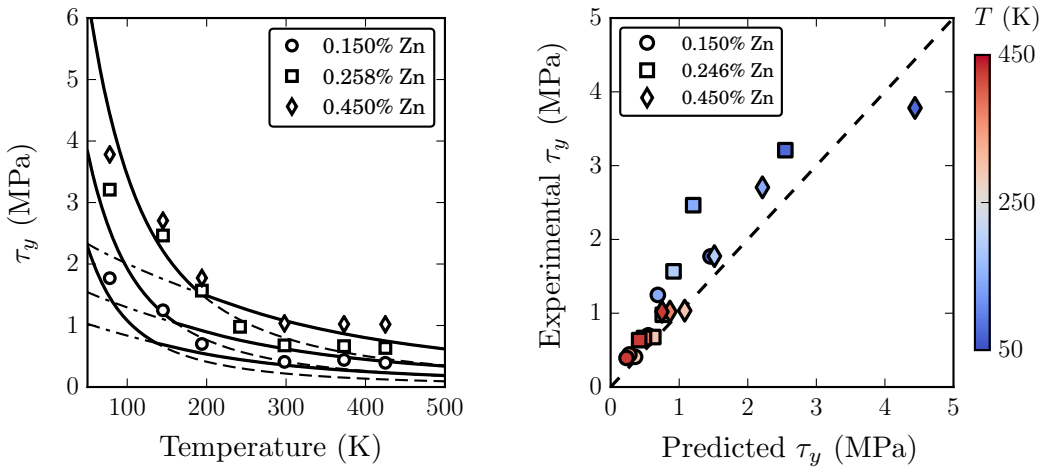

Figure 9: Experimental [84] and predicted finite temperature yield stress $\tau_y(T)$ for Mg-Zn alloys. Left: τ_y shown by the solid line, with the low and high temperature strengths shown by the dashed line (τ_{y1}) and dashed-dot line (τ_{y2}). Right: experimental versus predicted strength across all alloys and temperatures, with predictions using the self-consistent line tension Γ with scaling Eq. (36) by the ratio of Mg and Al shear moduli. Dashed line of slope of unity is a guide to the eye.

5.4. Twinning in Mg

The theory predicts how a dislocation will move in a random field of solutes. The dislocation is not restricted to be a lattice dislocation, and so equally applies, in principle, to dislocations along interfaces (with possible modifications needed for any finite Peierls stress). Thus, in particular, the model is applicable to the strengthening of twinning dislocations moving along a twin boundary, where the defect has a dislocation+step character. Our discussion here examines strengthening of the tensile twin dislocation in Mg due to Al and Zn solutes.

The solute/twin-dislocation interaction energies for Al solutes were computed using DFT and the dislocation pressure field, as shown in Fig. 1c. Notably, the solutes have a strong interaction (both positive and negative) with the twin boundary, independent of the twin dislocation. This new feature of the energetics emerges when studying dislocations moving along boundaries, but is not an impediment to application of the theory. Direct DFT calculations of the solute/twin-dislocation interaction energy are computationally very expensive, and so we computed Zn interactions with the twin boundary alone (no dislocation) and have then estimated the Zn interaction energy around the dislocation by a validated scaling of the corresponding values for Al [86]. The line tension is dominated by the step because the dislocation Burgers vector is quite small ($b \sim 0.5$Å). The line energy is computed as $\Gamma = 0.040$ eV.Å^{-1} from the twin dislocation core energy using the EAM Liu potential [87], which predicts twin boundary structure and energy, and twinning dislocation core structure, in good agreement with DFT [88].

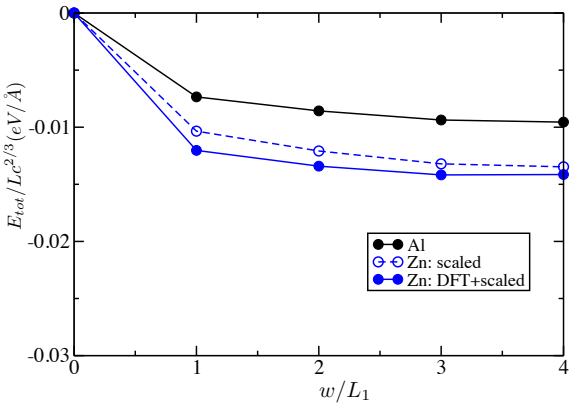

Figure 10: Normalized total energy change per unit length vs. roughening amplitude w normalized by the periodicity of the coherent twin boundary $L_1 = 7.58$Å, for Al and Zn solutes interacting with twinning dislocation in Mg. The Zn interaction energies are obtained by direct DFT calculations at selected sites and scaled Al interaction energies elsewhere. Use of the scaled energies at all sites (dashed line) introduces an error of ≈ 0.001 meV.Å^{-1} in the normalized total energy.

With the above inputs, the theory is applied. As found for Mg basal slip, application of the model

to the twinning problem shows new features, as follows. Fig. 10 shows the total energy per unit length of dislocation $\Delta E_{\rm tot}(w)/L$ for various values of the amplitude w. Unlike in the previous applications to lattice dislocations, a clear minimum in the total energy *does not emerge* from the analysis. Rather, the energy is almost independent of w, for each discrete (periodic) value of $w > 0$. This feature is unique to the twin dislocation because the interaction energies are dominated by the solute/*twin-boundary* energies rather than the solute/*twin-dislocation* energies. As the twin dislocation moves along the boundary plane, it shifts the twin boundary up by the unit step height and changes the relative positions of solutes with respect to the boundary; solutes on the original boundary are below the new boundary and solutes above the original boundary are on the new boundary. In a random solute field around the twin dislocation, the strengthening is dominated by the favorable statistical fluctuations of solutes along the original and new twin boundaries which extend beyond the defect core. Furthermore, the small line energy of the twin dislocation enables more bowing to find such favorable solute fluctuations. As a result, in the Mg twin, various roughening amplitudes w, given by multiples of the twin periodicity L_1, have nearly equal contributions to $\Delta\tilde{E}_p(w)$ and thus affect the total energy by comparable amounts.

Because there is no minimum in the total energy versus amplitude w, with all values of w having nearly equal energies, the analysis of strengthening for the twin dislocation is thus more complex than strengthening for the lattice dislocation but follows as a generalization of the two-minimum situation found in basal slip in Mg. For fixed values of temperature, concentration, and strain-rate, there are now many possible configurations available for the twinning dislocation to optimize its energy, *i.e.* the dislocation line may bow out by various multiples of L_1 towards favorable solute distributions. Among all of these configurations, the one requiring the highest stress to achieve the desired strain-rate at any given temperature is the configuration that controls the strengthening. Thus, a prediction of the yield stress versus temperature and concentration requires calculation of the strength for all possible roughening amplitudes w and then a determination of the maximum strength among all these strength values. The strength versus temperature at a given c and strain-rate is then constructed as the "envelope" of the strength vs. T curves for each possible integer bow out $w = nL_1$. Creation of the envelope is straightforward but unwieldy. Since $\Delta E_{\rm tot}/(Lc^{2/3})$ is essentially constant for all the integer values of $w = nL_1$ (see Fig. 10), we can develop an analytic model by considering w as a continuous variable for $w \geq L_1$ but with $\Delta E_{\rm tot}/(Lc^{2/3})$ independent of w, and carry out the maximization analytically. This yields an analytic expression for the finite-T, finite strain-rate yield stress (for $w \geq L_1$) given by

$$\tau_y(T,\dot{\epsilon}) = \frac{2\pi(33-8\sqrt{2})}{25\sqrt{5}b}\frac{[-\Delta E_{\rm tot}/Lc^{\frac{2}{3}}]^{\frac{3}{2}}\Gamma^{\frac{1}{2}}c}{k_BT\ln\dot{\varepsilon_0}/\dot{\varepsilon}}, \quad (39)$$

where $\Delta E_{\rm tot}/(Lc^{2/3})$ is the computed constant value for $w \geq L_1$ shown in Fig. 10 for the given solute. This analytic result is in excellent quantitative agreement with the results obtained through numerical construction of the "envelope" of strength vs. T curves. The analytic result, encompassing all possible bow outs, changes the scaling of strength versus concentration and temperature, as compared to the case for lattice dislocations. For the twin, the strength is directly proportional to concentration c and inversely proportional to the temperature T.

We now compare the model to experiments for the Mg-Al-Zn alloys. For multiple solute types at dilute concentration, the above model can be generalized to

$$\tau_y(T,\dot{\epsilon}) = \frac{2\pi(33-8\sqrt{2})}{25\sqrt{5}b}\frac{\Gamma^{\frac{1}{2}}\sum_n c_n[-\Delta E_{{\rm tot},n}/Lc_n^{\frac{2}{3}}]^{\frac{3}{2}}}{k_BT\ln\dot{\varepsilon_0}/\dot{\varepsilon}} \quad (40)$$

where n ranges over the solute types (but not the host matrix). The predictions use the relevant collective solute/twin-dislocation interaction energy quantity $\Delta E_{\rm tot}/(Lc^{2/3})$, computed using the DFT-computed solute/twin-dislocation interaction energies. Specifically, we use the average values of $\Delta E_{\rm tot}/(Lc^{2/3}) = -0.009$ meV.Å^{-1} for Al and -0.014 meV.Å^{-1} for Zn, corresponding to the average values as indicated in Fig. 10. We compare to experiments performed at T=300K and $\dot{\varepsilon} = 10^{-3}$s^{-1}, and use a reference strain-rate of $\dot{\varepsilon}_0 = 10^5$s^{-1}. Twinning in pure single-crystal Mg was studied by Kelly and Hosford [89], who obtained a strength of 3 MPa at room temperature; this value represents the "Peierls stress" for twinning and must be added to our prediction in making any comparison with experiments. Direct and systematic experiments measuring the strengthening effect of solutes on twinning in Mg alloys have

not been reported. However, there is significant stress-strain data on textured polycrystals with either controlled solute concentrations or commercial compositions, and these studies have been used to estimate the stresses needed to drive twinning. Ref [90] contains an analysis of earlier experimental data for AZ31 [91, 92, 93, 94], AZ61 and AZ80 [92] at various grain sizes. The twinning yield stress for these alloys can be determined from the results at a (large) grain size of 100 μm and applying the appropriate Schmid factor (m = 0.37) [90]. The experimental strengths and our predictions for the total twin yield stress (CRSS) including the Peierls barrier are shown in Table 3; the agreement is very good. Estimates of the critical resolved shear stress (CRSS) required for twin growth in Mg AZ31 alloys were also reported to be in the range of 6-14 MPa [95], in reasonable agreement with the prediction of $\tau_y = 14$ MPa. However, Stanford and Barnett [90] studied the solute strengthening of twinning in binary Mg-Zn polycrystals and found that the CRSS is independent of Zn concentration up to 1 at% (2.8 wt%), in disagreement with our prediction that the strength should increase from the Peierls stress of 3 MPa to ≈ 8 MPa at 1 at% Zn. These strengthening levels are small, but should be measurable if real. The ratio of twin vs. basal CRSS predicted by the model, however, reproduces well the ratio obtained in Ref. [90].

Table 3: Twinning yield stress in MPa for commercial Mg alloys, as measured and as predicted by the present model. The compositions used in the model are shown.

Alloy	c ($at\%$)	Ref. [90]	This work
AZ31	Al:2.7, Zn:0.37	18	14
AZ61	Al:5.47, Zn:0.37	22	23
AZ80	Al:7.28, Zn:0.187	33	28

Overall, the theory cannot match two entirely different experimental results, those on the Mg-Al-Zn alloys and those on the binary Mg-Zn alloys. The expected uncertainties in the model predictions (due to line energy and solute/twin interaction energies) are not large enough to rectify the discrepancy. We consider the good agreement found for the AZ alloys to suggest that solute strengthening of twinning does exist, and with the theory pointing toward these experiments as more representative. The issue of strengthening of twinning by solutes will be resolved experimentally only through designed tests on single-crystal Mg alloys, although such studies may be complicated by the need to nucleate twins. Nonetheless, our robust mechanistic theory provides a theoretical foundation for interpretation of such future results.

5.5. fcc High Entropy Alloys

Finally, we consider the case of multi-component High Entropy Alloys (HEAs). We view these materials simply as specific cases of non-dilute random solid solutions, making our general theory applicable. A recent effort treating HEAs as random solid solution alloys was made by Toda-Caraballo and Rivera [71]. They assumed a dilute-limit Labusch-type analysis plus a separate double-kink thermal activation model, and used generalized size and modulus misfit parameters to fit existing data, followed by a data-analytics-type approach to estimate strengths of HEAs. The recent experimental work carried out on fcc HEAs by Wu *et al.* [96] showed that the measured activation volumes are much larger than those typical for kink-pair mechanisms, and that the Labusch-type analysis of Ref. [71] was qualitatively compatible with the experimental strenghs. The derived theory for arbitrary composition random solid solutions presented here, when reduced to the elastic limit (Eqs. (25) and (26)), leads to functional forms for strength and energy barrier having similarities to those assumed by Toda-Caraballo and Rivera, and thus puts the problem on a firm theoretical foundation.

Here, we apply the solute strengthening model to several fcc HEAs in the Ni-Co-Fe-Cr-Mn family. In the detailed publication [61], comparison of the theory to molecular simulations on a model Ni-Fe-Cr alloy, using EAM interatomic potentials, was presented to validate important features of the theory. Here, we concentrate on predictions for real materials. The Ni-Co-Fe-Cr-Mn family has been well-studied by George and coworkers [97, 98, 99], who performed uniaxial tensile yield strengths versus temperature, strain-rate, and grain size d_g in polycrystalline materials. The HEA strengths showed two contributions: a grain-size-dependent Hall-Petch (H-P) contribution $\sigma_{\mathrm{H-P}}(d_g)$ and a chemical/alloying effect σ_{alloy} that is modeled by solute strengthening theory. For comparison with theoretical predictions, we thus only consider those alloys for which the measured H-P contribution can be subtracted from the total experimental strength, *i.e.* NiCoFeCr and NiCoFeMn alloys at various temperatures [97, 99], and NiCo, NiFe, NiCoFe, and NiCoCr alloys at $T = 293K$ [98] (for details see Ref. [61]).

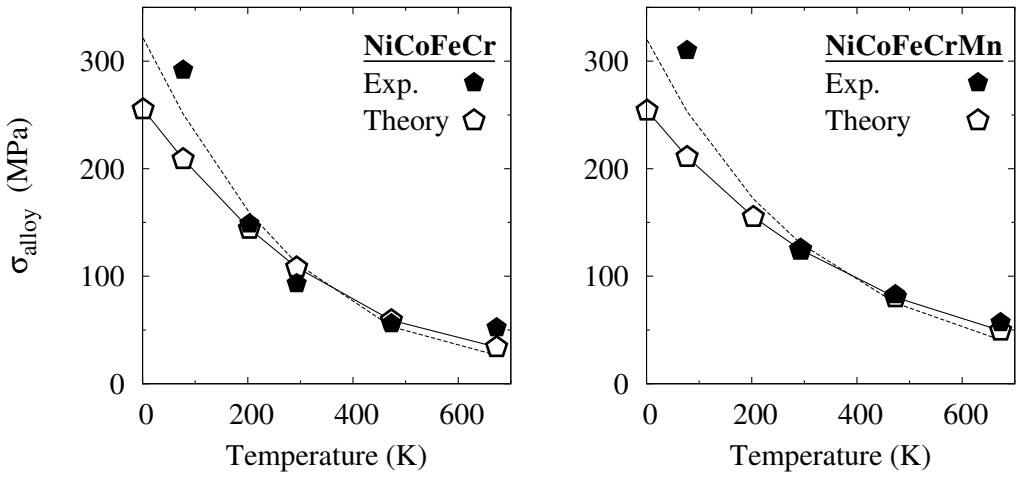

Figure 11: Quantitative comparison between experimental and theoretical yield stress versus temperature for the NiCoFeCr (left) and NiCoFeCrMn (right) equiatomic alloys [97, 99], as measured (black symbols) after subtraction of the Hall-Petch contribution to the strength and as predicted by the theory (open symbols). The dashed lines show predictions using a line tension of one-half the original value (*i.e.* α is reduced by 1/2), showing the weak sensitivity of the model to the line tension except at very low T.

Prediction of $\sigma_{\rm alloy}$ for these alloys requires the input parameters of the model. *Ab initio* computed data are not available, and are also very challenging to obtain in these highly-concentrated, multicomponent systems. We therefore use the simplified elasticity model of Eqs. (25) and (26). Measurements of the polycrystalline elastic constants (μ, ν) versus temperature (for NiCoFeCr and NiCoFeCrMn) and at room temperature (for NiCo, NiCoFe, and NiCoCr) [97, 99] and Burgers vectors b are available. The average misfit volume $\Delta\overline{V}_n$ of each solute element is computed using literature data on the lattice parameter of binary Ni-X (X=Co, Cr, Fe) fcc solid solutions [60, 100, 101] and on the wider family of Ni-Co-Fe-Cr-Mn HEAs studied by Wu *et al.* [97], and applying Vegard's law to the atomic volumes [61]. The corresponding atomic volumes for each element are shown in Table 4, and the misfit volume of solute type n in any alloy is then computed as $\Delta\overline{V}_n = V_n - \overline{V}$. The line tension parameter $\alpha = 0.123$ is obtained from the atomistically-measured edge dislocation line tension in the EAM FeNiCr effective matrix, and is close to the coefficient for elemental Al [83]. The dislocation cores in HEAs show large dissociation distances $d > 10b$, consistent their relatively low stacking fault energies $\gamma_{\rm SF}$ (low *ab initio* estimates, and large stacking fault ribbons observed experimentally [102, 103, 104]). The minimized parameters of Eqs. (26) and (25), $f_1(w_c) \sim 0.35$ and $f_2(w_c) \sim 5.7$ for the low temperature solution (which is the only one relevant for these materials up to $\sim$ 700K) are thus independent of the precise value of d or $\gamma_{\rm SF}$.

Table 4: Atomic volumes V_n of element n =Ni, Co, Fe, Cr and Mn, computed from litterature data on the experimental lattice parameters of Ni-X binary solid solutions for X=Co, Fe and Cr [60, 100, 101] and on the wider family of Ni-Co-Fe-Cr-Mn HEAs [97], and applying a Vegard's law to the average alloy atomic volume.

n	Ni	Co	Fe	Cr	Mn
V_n (Å^3)	10.94	11.12	12.09	12.27	12.60

With all these inputs, the analytic theory of Eqs. (25) and (26) then predicts the strength versus temperature and strain-rate for any alloy composition. Figs. 11a,b show the predicted and measured alloy contributions $\sigma_{\rm alloy}$ to the yield stress for the NiCoFeCr and NiCoFeCrMn alloys over the complete temperature range at $\dot{\varepsilon} = 10^{-3}$ s^{-1}. The predictions are very good, again with no fitting parameters. The NiCoFeCr and NiCoFeCrMn alloy strengths are nearly identical, which the theory attributes to the compensating effects of a larger mis-

fit contribution for NiCoFeCrMn and a larger μ for NiCoFeCr. The predictions at the lowest temperature ($T = 77K$) are, however, well below the experiments. This could be due to chemical-specific core interactions that are absent in the elasticity model, or to the neglected fluctuations due to local structural and chemical disorder in HEAs (appearing in Eq. (8)). On the other hand, Figs. 11a,b also show predictions using a line tension parameter $\alpha = 0.06125$, demonstrating that the strength predictions are nearly independent of line tension except at $T = 77K$ and thus some of the discrepancy at $T = 77K$ could be due to inaccuracy of the line tension. Comparison of parameter-free theory and experiment for four other alloys (NiCo, NiFe, NiCoFe, NiCoCr) [98] at $T = 293K$ are shown in Fig. 12, and again the overall agreement is very good, with accuracy levels similar to those achieved in the simpler dilute binary alloys [17, 18]. The theory also preserves the observed ordering of strength versus composition, with the ternary NiCoCr alloy having the highest strength, for instance.

In addition to the good quantitative agreement with experiments, the theory answers many open questions about strengthening in HEAs: (i) strength does not directly depend on the number of components N, and is not necessarily maximized by the equi-atomic composition, (ii) the strongest and most temperature-insensitive materials are achieved by maximizing the concentration-weighted mean-square misfit volume quantity and/or increasing the shear modulus, and (iii) the stacking fault energy has little influence on strength. These insights provide a basis for computationally-guided design of higher-strength many-component random alloys. This is discussed further below.

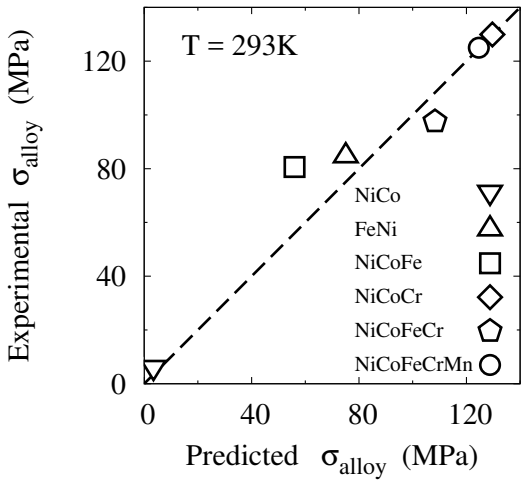

Figure 12: Experimental [97, 98, 99] versus predicted strengths for several HEAs in the Ni-Co-Fe-Cr-Mn family at $T = 293K$, after subtraction of the Hall-Petch contribution to the strength. The dashed line of slope of unity is a guide to the eyes.

6. Discussion

The new strengthening model presents possibilities for alloy design while pointing to additional topics for future work. We discuss these issues here.

6.1. Identification of promising materials

Having demonstrated that the present model is robust and predictive, the identification of new promising materials becomes reachable. The full theory does not have any adjustable parameters; all inputs - elastic constants, Burgers vector, and the more complex line tension, dislocation core structure, and solute/dislocation interactions - can, in principle, be computed. If computed from reliable *ab initio* methods, then systematic exploration of compositional phase space, through high-throughput computing of model inputs accompanied by application of the model to predict strength, will allow for the creation of "design maps" for new materials. Such an approach is then coupled with predictions of alloy phase stability through well-established thermodynamic modeling.

For dilute alloys, *ab initio* computation of dislocation core structure and solute/dislocation interaction is accessible with high accuracy, as described in the partner Overview article [25]. The line tension is computable from either empirical potential simulations (given good interatomic potentials) or from DFT-parameterized line tension models [83, 105]. New alloy design can therefore be undertaken based on the full version of the strengthening model of Eqs. (8), (12) and (14).

For non-dilute alloys such as HEAs, the problem is more complex due to the high number of components and the chemical, structural, and possible magnetic disorder in such materials. However, the model here, using an effective matrix material and including first-order local fluctuations around the average, provides a formal baseline. Properties of the effective matrix and disor-

der are challenging for *ab initio* calculations, but techniques such as the Virtual Crystal Approximation [62] and the Coherent Potential Approximation [63, 64, 106, 107, 108], and the use of Special Quasi Random structures [109, 110] provide directions for progress. Direct calculations of average properties, such as C_{ij}, b, $\Delta\overline{V}_n$, $\sigma^2_{\Delta V_n}$, and $\gamma_{\rm SF}$ are currently feasible (see Refs. [102, 103]) and provide the inputs needed for application of the simplified elasticity model. The precise dislocation core structure, direct solute/dislocation core interactions $U^n(x_i, y_j, z_k)$, and dislocation line tension, are all far more challenging, and perhaps prohibitively expensive, to compute. However, well-validated empirical potentials for alloys, tuned using DFT inputs, may allow all model inputs to be computed with reasonable accuracy [60, 65]. The availability of such potentials is not sufficient at the present time, however. Thus, *ab initio*-based design is likely best pursued using the elasticity-based model (Eqs. (24)-(26)) with dislocation structures parameterized by b, $\gamma_{\rm SF}$ and $\gamma_{\rm USF}$, and a line tension scaled by μb^2. Within this simplified elasticity model, higher strengths will generally be obtained for a larger solute misfit parameter $\left[\sum_n c_n \left(\Delta\overline{V}_n^2 + \sigma^2_{\Delta V_n}\right)\right]^{1/2}$ and/or larger μ, with $\gamma_{\rm SF}$ of less importance. New alloys designed using the elasticity-based theory with computable material inputs will, while not exact, provide a clear physical framework for identifying promising compositions to achieve higher-performance HEAs, austenitic stainless steels, etc.

6.2. Failures of the theory

The present theory has been shown to be quantitatively predictive across a range of systems. However, as mentioned earlier in section 5, the theory fails for very dilute Al-Fe binary alloys strength [17]. The DFT computations for Fe/dislocation interaction energies are similar to, albeit slightly larger than, the results for Al-Mn [17]. The measured strengths of Al-Fe at Fe contents of 10-50 ppm are, while small, roughly 10 times larger than predicted by the theory. Analysis of the DFT provides no insights into the reasons for this failure of the theory. Ma *et al.* [76] analized the specific role of the screw dislocations in these Al-Fe alloys, but this could not resolve the discrepancy with the experimental results. Investigations into other possible effects (e.g. interaction of Fe with O or other impurities, formation of strong Fe-Fe pairs, etc. see further discussions in subsection 6.6) remains to be done. As a practical matter, we have fit the theory to the Al-Fe binary response to obtain fitted values for $\Delta E_b/c^{1/3}$ and $\tau_{y0}/c^{2/3}$, and have then used these parameters to successively predict strengths in nominal binary alloys that contain Fe at tens of ppm levels by treating them as ternary alloys (Al-Cu-(Fe), Al-Cr-(Fe), commercial Al-Mg-(Fe)). Nonetheless, the failure of the theory in this one case shows that the strengthening mechanism envisioned in the theory may not be applicable even when first-principles DFT results do not indicate any anomalous behavior in the solute/dislocation interaction energies.

6.3. Contribution of screw dislocations to solute strengthening

In the present model, the alloy strength has been predicted while focusing only on the energetics and motion of the edge dislocation. Atomistic simulations using EAM potentials show comparable interaction energies and/or zero-temperature strengths for screw and edge dislocations in fcc solid solution Ni-Al [38] and Al-Mg alloys [82, 111]. Such results cannot be expected from usual elasticity theory describing the screw pinning by a modulus misfit and the edge pinning by a dominant size misfit. For low solute concentration, the strengthening of the screw effect is clearly a consequence of the dissociation of the screw dislocation core into Shockely partials that each have edge components. Yasi. *et al.* [39] computed the solute/dislocation interactions of solutes with basal edge and screw dislocations in hcp Mg, and found them comparable in magnitude. These initial findings are consistent with TEM observations of dislocation microstructures in fcc materials showing them to be fairly isotropic [20], *i.e.* having equal proportion of edge and screw dislocation segments.

The present theory does not exclude screw dislocations from consideration, and thus can be applied to screw dislocations. This was nicely pursued by Ma *et al.* [76], who showed that the strengthening of the screw dislocation in Al was indeed fairly comparable to that of the edge. This result would seem surprising at first, since the screw dislocation has no long-range pressure field to interact with the solute misfit volume. However, the dissociation of the screw dislocation core creates a pressure field due to the edge component of the partials. In addition, three other factors are important in the quantitative magnitude of the strengthening: w_c,

Γ, and the Peierls stress. First, the line tension for the screw dislocation is much larger than that for the edge, and this increases the energy barriers for screw motion (see Eq. (12)). Second, the screw core is also less dissociated than the edge core, and in Al we expect w_c to scale with the partial separation (because the partial separation is small), and the strength increases with decreasing w_c. Third, the zero-temperature Peierls stress of fcc dislocations tends to be somewhat larger than that of the edge, and this also reduces the difference in strengthening between edge and screw. Full computations for the screw dislocation in fcc Al alloys [76] show that, in general, the energy barrier ΔE_b for the edge is about twice that observed for the screw while the zero-temperature flow stress τ_{y0} is smaller than that for the screw dislocation. Although the line connectivity of the edge and screw should provide some averaging of the individual mobilities, there is no clear approach for combining edge and screw strengths versus temperature and strain rate. But with the edge strength being larger under most practical conditions, we expect the edge strengthening to control the overall strength. However, further investigations of the respective role of edge and screw dislocations remain of high interest.

6.4. Strengthening in other materials

The model presented in the paper is also applicable to interstitial solid solutions in low-Peierls stress alloys, provided the dislocation core structure is not too strongly modified by the solute(s). A few complications arise, as such properly enumerating all the possible solute sites, accounting for the interactions between the deviatoric misfit strains (due to, e.g., tetragonal distortions generated by interstitial solutes) and the deviatoric dislocation stress field, and accounting for the various orientations of such configurations. Recent work presents some analysis of these issues in the context of Hydrogen in Ni [112], but in general the complications present no theoretical or conceptual difficulties.

In materials such as bcc alloys, the Peierls stress of the pure material (or the effective matrix material) is high. Thus, solutes can soften and strengthen, and various models have been developed to account for the role of solutes on the temperature and strain-rate dependent motion of dislocations in these materials [20, 113]. However, remaining within the generally-accepted kink-pair nucleation model for screw motion in bcc materials, the present theory points toward another possible avenue for analysis of the solute strengthening/softening, particularly in non-dilute alloys. This is a topic for future work.

We also remind ourselves that an underlying assumption of the present class of models is that solutes do not significantly distort the dislocation core structure of the matrix material (or effective matrix) [8, 9, 10]. When such large distortions do occur, they are accompanied by large reductions in the system energy, e.g. large solute/dislocation interaction energies. If in addition there are no long-range interactions, the "strong pinning" Fleischer-Friedel models may become operative. One example of such a case is the high strengthening effect of dilute oxygen in hcp titanium, well-established experimentally. Yu et al. [10] have recently shown that an individual O in the very core of the dislocation provides much stronger pinning than that of the collective effect of the surrounding solutes (no long-range elastic interactions). Application of the classical Fleischer-Friedel model using the DFT-estimated parameters provides predictions in the range of the measured experimental values, although the measurements were performed in nanopillars and thus include a significant pillar size effect. Thus, continued development of point-pinning models, especially for thermal activation and at realistic solute concentrations, is valuable.

6.5. Flow stress in atomistic simulations

Direct modeling of solute strengthening by Molecular Dynamics (MD) simulations is tempting but not obvious. Direct MD simulations cannot capture the evolution of very long, wavy dislocations ($L \gg \zeta_c$), having energy barrier of the order of 0.7-1.1eV, at typical experimental strain-rates. Instead, we advocate the study of single segments of length $\zeta \sim \zeta_c$. At this length, the dislocation remains straight as it move through the field of solutes. The corresponding theory in this case is slightly different but remains analytical. We used this approach for model Fe-Ni-Cr alloys modeled with an EAM potential [114] and demonstrated good agreement between direct simulations and model predictions [61]. While care must be taken, such studies validate crucial aspects of the theory such as the internal length scale w_c and average flow stress versus alloy composition.

Nonetheless, numerical simulations of solute strengthening have, however, led to the identification of important trends and understandings.

We already mentioned above the rather comparable role of the screw and edge dislocations in strengthening found in MD simulations using empirical potentials [38, 82, 111]. The contribution to the strength of solutes in planes away from the glide plane has also been identified through atomistic simulations in Al-Mg and Ni-Al systems [37, 38, 82, 111, 115]. This clearly established that the historical approaches that only included solutes in the glide plane were to be revised. Furthermore, the specific strengthening due to solute pairs when the solute concentration increases (and with the reference taken as the pure elemental matrix) has been measured [38, 115]. MD simulations also showed a finite size effect in solute strengthening [111, 37, 116], *i.e.* the dependence of the measured flow stress on both the dislocation line length and the glide distance, due to the statistical nature of the solute configuration. This was extensively studied using simplified line-tension-based numerical models [37, 117]. When correctly parameterized using atomistic information [37], such models reproduce MD simulations at zero-temperature for given dislocation length and glide distance. However, the approach remains numerical and the thermal activation is yet to be included. In general, further work to understand the ability and/or limitation of direct MD simulations to determine the strengths relevant to real materials remains a fruitful area.

6.6. Alloys with Short Range Order

A strong assumption in both historical models and the strengthening model presented in this paper is the representation of the solid solution as a random alloy. Although this can be a good approximation for some alloys (e.g. in HEAs [118]), short range order (SRO), *i.e.* correlations between the chemical occupancy of the atomic sites, can exist in materials. Evidence of SRO effects on strength has been experimentally demonstrated for instance in NiAl fcc solid solution alloys [119, 120]. As compared to the fully random case, SRO affects the strength in two different ways: modified statistics and existence of non-negligible solute/solute interactions. These factors can introduce additional softening/strengthening effect [119, 121, 122]. Inclusion of SRO can be performed within the framework of the current model, in principle. A more-complex energetic model is required, and appropriate treatment of the statistics in the short-range-ordered solid solution is challenging [123], but the current model provides the baseline to include those effects.

7. Summary

In this overview, we have summarized the extensive recent progress within the Labusch-type weak-pinning model for solid solution strengthening for metallic alloys, accounting for multiple solutes at arbitrary composition [17, 61, 68, 69]. The detailed model makes contact with both historical models and recent developments. Most importantly, the model provides many insights about the physics of the strengthening. These insights extend to rather subtle issues, including (i) identifying conditions under which stress equivalency is upheld, (ii) providing a clear physical origin of the observed high-T "plateau", (iii) demonstrating which materials parameters are the key quantities for strengthening, (iv) the relatively unimportant role of stacking fault energy, and (v) the role of additional fluctuations in local solute energies due to local chemical environments. Application of the model to low-Peierls stress materials shows its predictive capacity, for both dilute and concentrated alloys. These validations, each revealing some new features, open the way for design of optimized solute-strengthened alloys. The model also provides a baseline to consider short-range ordering effects, interstitial solutes (if they do not modify strongly the dislocation core structure), and other crystallographic structures, all of which will be pursued in future work.

Acknowledgments

Support for this work was provided through a European Research Council Advanced Grant, "Predictive Computational Metallurgy", ERC Grant agreement No. 339081 - PreCoMet.

Appendix A. Role of the dislocation core structure

In the various applications shown in this paper, we have seen that the dislocation core structure is important, and this has been raised by other authors [39, 76]. To study its influence, we thus parameterize the Burgers vector distribution along the glide plane by two Gaussian peaks, each of standard

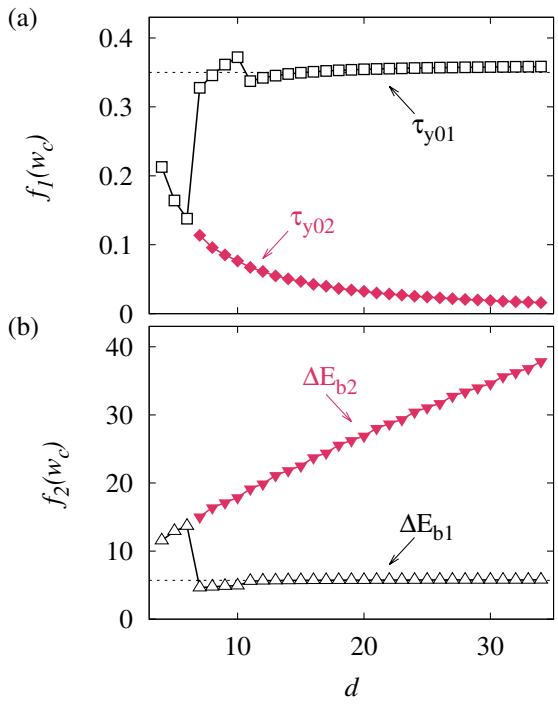

Figure A.13: Minimized dislocation structural coefficients (a) $f_1(w_c)$ for zero-temperature strength τ_{y0} appearing in Eq. (25), and (b) $f_2(w_c)$ for the energy barrier ΔE_b appearing in Eq. (26), vs. d the dissociation distance of an fcc edge dislocation, related to $\gamma_{\rm SF}$ and isotropic elastic constants through the elasticity relation $d = \mu b(2+\nu)/(24\pi(1-\nu)\gamma_{\rm SF})$.

deviation σ, separated by a stacking fault of width d, as follows

$$\frac{\Delta b(x_i)}{b} = \frac{e^{-\frac{1}{2}\left(\frac{x_i-d/2}{\sigma}\right)^2} + e^{-\frac{1}{2}\left(\frac{x_i+d/2}{\sigma}\right)^2}}{\sum_{k=-\infty}^{+\infty} e^{-\frac{1}{2}\left(\frac{x_k-d/2}{\sigma}\right)^2} + e^{-\frac{1}{2}\left(\frac{x_k+d/2}{\sigma}\right)^2}}, \tag{A.1}$$

where $x_i = nb/2$ with $n = 0, \pm1, \pm2...$ is the position along the glide plane. Atomistic studies of fcc dislocations in various materials (Al, Ni, Fe-Ni-Cr alloys) showed that typical σ values range from $1.25b$ to $2.5b$, and scale with $\mu b^2/\left(4\pi(1-\nu)\gamma_{\rm USF}\right)$, with $\gamma_{\rm USF}$ the unstable stacking fault energy [61]. Fixing $\sigma = 1.5b$, the dimensionless pressure field $f(x_i, y_j)$ can then be computed, and the minimized quantities in brackets in Eqs. (25) and (26) are calculated versus d, as shown in Fig.A.13. Isotropic elasticity [40] yields $d = \frac{\mu b^2}{\gamma_{\rm SF}} \frac{(2+\nu)}{24\pi(1-\nu)}$ for an edge dislocation.

When both gaussian peaks are well separated, *i.e.* when $d > 10b$, there are two minimum energy configurations leading to two different minimized coefficients for both zero-temperature stress and energy barrier. The first minimized core coefficients in Eqs. (25) and (26) associated to τ_{y01} and ΔE_{b1}, are nearly independant of d. For typical elastic moduli, the strength is thus independent of $\gamma_{\rm SF}$ for $\gamma_{\rm SF} < 100$ mJ/m^2. The second minimum energy configuration, associated to a larger w_c, with low τ_{y02} and high ΔE_{b2}, provides a "plateau" stress relevant only at very high temperatures, which appears to be more sensitive to the exact value of the stacking fault energy (see the former discussion on Mg alloys). For low-to-intermediate temperatures, the simplified theory of Eqs. (25) and (26) with coefficients $f_1(w_c) \simeq 0.35$ and $f_2(w_c) \simeq 5.7$ is fully *analytic* and predictions require only elastic moduli, lattice constants, and misfit volumes versus alloy composition. This is valid for low stacking fault energy materials, such as fcc high entropy alloys, austenitic stainless steels, or cupper alloys, for instance. When $d < 10b$ on the other hand, the two gaussian peaks in the Burgers vector distribution start to overlap. The minimized core coefficients are not independant of d anymore, and thus the exact value of γ_{SF} matters for both core coefficients in τ_{y0} and ΔE_b, for all the range of temperature. As it can be seen in Fig. A.13, there is a transition between a regime having two minimum energy configurations and only one minimum energy configuration (like in Al alloys).

This simple model of two gaussian peaks for the Burgers vector distribution of the dissociated dislocation allows us to understand the exact role of the stacking fault energy in predicting the strength and its temperature evolution. Other mathematical expressions could be used to parameterize the Burgers vector distribution, like the Peierls-Nabarro description [26], or discrete spread-core models [17]. They would lead to the same conclusions about the importance of the dissociation distance on the alloy strength.

References

References

[1] J. R. Davis, Aluminium and Aluminium Alloys, ASM International, Materials Park, Ohio, 1993.

[2] M. F. McGuire, Stainless Steels for Design Engineers, ASM International, Materials Park, Ohio, 2008.

[3] S. Kang, P. K. Domalavage, N. J. Grant, Mechanical properties of rapidly solidified modified cupro-nickel alloys, Mater. Sci. Eng. 78 (1986) 33–44.

[4] X. Mao, F. Fang, J. Jiang, R. Tan, Effect of annealing on microstructure and properties of Cu-30Ni alloy tube, J. Mater. Process. Technol. 209 (2009) 2145–2151.

[5] M.-H. Tsai, J.-W. Yeh, High-entropy alloys: A critical review, Mater. Res. Lett. 2 (3) (2014) 107–123. doi:10.1080/21663831.2014.912690.

[6] Y. Zhang, T. T. Zuo, Z. Tang, M. C. Gao, K. A. Dahmen, P. K. Liaw, Z. P. Lu, Microstructures and properties of high-entropy alloys, Prog. Mater. Sci. 61 (2014) 1–93. doi:10.1016/j.pmatsci.2013.10.001.

[7] B. Gludovatz, A. Hohenwarter, D. Catoor, E. H. Chang, E. P. George, R. O. Ritchie, A fracture-resistant high-entropy alloy for cryogenic applications, Science 345 (6201) (2014) 1153–1158. doi:10.1126/science.1254581.

[8] L. Ventelon, B. Lüthi, E. Clouet, L. Proville, B. Legrand, D. Rodney, F. Willaime, Dislocation core reconstruction induced by carbon segregation in bcc iron, Phys. Rev. B 91 (2015) 220102. doi:10.1103/PhysRevB.91.220102.

[9] T. Tsuru, D. C. Chrzan, Effect of solute atoms on dislocation motion in Mg: An electronic structure perspective., Sci. Rep. 5 (2015) 8793. doi:http://doi.org/10.1038/srep08793.

[10] Q. Yu, L. Qi, T. Tsuru, R. Traylor, D. Rugg, J. W. Morris, M. Asta, D. C. Chrzan, A. M. Minor, Origin of dramatic oxygen solute strengthening effect in titanium, Science 347 (6222) (2015) 635–639. doi:10.1126/science.1260485.

[11] N. Chaari, Modélisation ab initio de la plasticité dans les métaux hexagonaux purs, Zr et Ti, et effet de l'oxygène., Ph.D. thesis, INP Grenoble, France (2015).

[12] R. Bullough, R. C. Newman, The kinetics of migration of point defects to dislocations, Rep. Prog. Phys. 33 (1970) 101–148. doi:10.1088/0034-4885/33/1/303.

[13] E. Clouet, S. Garruchet, H. Nguyen, M. Perez, C. S. Becquart, Dislocation interaction with C in α-Fe: A comparison between atomic simulations and elasticity theory, Acta Mater. 56 (2008) 3450–3460. doi:10.1016/j.actamat.2008.03.024.

[14] E. Clouet, L. Ventelon, F. Willaime, Dislocation core field: II. screw dislocation in iron, Phys. Rev. B 84 (2011) 224107. doi:10.1103/PhysRevB.84.224107.

[15] E. Hayward, C. Deo, B. P. Uberuaga, C. N. Tomé, The interaction of a screw dislocation with point defects in bcc iron, Philos. Mag. 92 (2012) 2759. doi:10.1080/14786435.2012.674646.

[16] E. Clouet, The vacancy - edge dislocation interaction in fcc metals: a comparison between atomic simulations and elasticity theory, Acta Mater. 54 (2006) 3543–3552. doi:10.1016/j.actamat.2006.03.043.

[17] G. P. M. Leyson, L. G. Hector Jr., W. A. Curtin, Solute strengthening from first principles and application to aluminum alloys, Acta Mater. 60 (9) (2012) 3873 – 3884. doi:http://dx.doi.org/10.1016/j.actamat.2012.03.037.

[18] G. P. M. Leyson, L. G. Hector Jr., W. A. Curtin, First-principles prediction of yield stress for basal slip in Mg–Al alloys, Acta Mater. 60 (13–14) (2012) 5197 – 5203. doi:http://dx.doi.org/10.1016/j.actamat.2012.06.020.

[19] J. D. Eshelby, The determination of the elastic field of an ellipsoidal inclusion, and related problems, Proc. Roy. Soc. Lond. A 241 (1957) 376–396. doi:10.1098/rspa.1957.0133.

[20] A. Argon, Strengthening Mechanisms in Crystal Plasticity, Oxford Univ. Press, 2007.

[21] H. Suzuki, The yield strength of binary alloys, in: Dislocations and Mechanical Properties of Crystals, New York ; Wiley, 1956, p. 363.

[22] C. Woodward, S. I. Rao, Flexible ab initio boundary conditions: Simulating isolated dislocations in bcc Mo and Ta, Phys. Rev. Lett. 88 (2002) 216402. doi:10.1103/PhysRevLett.88.216402.

[23] E. Clouet, L. Ventelon, F. Willaime, Dislocation core energies and core fields from first principles, Phys. Rev. Lett. 102 (2009) 055502. doi:10.1103/PhysRevLett.102.055502.

[24] X. Zhang, G. Lu, W. A. Curtin, Multiscale quantum/atomistic coupling using constrained density functional theory, Phys. Rev. B 87 (2013) 054113. doi:10.1103/PhysRevB.87.054113.

[25] D. Rodney, E. Clouet, L. Ventelon, D. R. Trinkle, L. Pizzagalli, F. Willaime, *Ab initio* modeling of dislocation core properties, Acta Mater., in preparation.

[26] V. V. Bulatov, W. Cai, Computer Simulations of Dislocations, Oxford series on materials modelling, Oxford University Press, 2006.

[27] J. Friedel, Dislocations, Pergamon Press, Oxford, 1964.

[28] R. Fleischer, Solution hardening, Acta Metall. 9 (11) (1961) 996 – 1000. doi:http://dx.doi.org/10.1016/0001-6160(61)90242-5.

[29] R. L. Fleischer, Substitutional solution hardening, Acta Metall. 11 (1963) 203–209. doi:10.1016/0001-6160(63)90213-X.

[30] N. F. Mott, F. R. N. Nabarro, Dislocation theory and transient creep, Phys. Soc. Bristol Conf. Rep. (1948) 1–19.

[31] N. F. Mott, A theory of work-hardening of metal crystals, Philos. Mag. 43 (1952) 1151–1178. doi:10.1080/14786441108521024.

[32] R. Labusch, A statistical theory of solid solution hardening, Phys. Stat. Sol. A 41 (2) (1970) 659. doi:10.1002/pssb.19700410221.

[33] R. Labusch, Statistische theorien der mischkristallhärtung, Acta Metall. 20 (7) (1972) 917 – 927. doi:http://dx.doi.org/10.1016/0001-6160(72)90085-5.

[34] F. R. N. Nabarro, The statistical problem of hardening, J. Less-Common Metals 28 (2) (1972) 257 – 276. doi:http://dx.doi.org/10.1016/0022-5088(72)90129-4.

[35] L. Proville, D. Rodney, M.-C. Marinica, Quantum effect on thermally activated glide of dislocations, Nat. Mater. 11 (10) (2012) 845–849. doi:10.1038/nmat3401.

[36] G. P. M. Leyson, W. A. Curtin, Friedel vs. Labusch: the strong/weak pinning transition in solute strengthened metals, Philos. Mag. 93 (19) (2013) 2428–2444. doi:10.1080/14786435.2013.776718.

[37] L. Proville, S. Patinet, Atomic-scale models for hardening in fcc solid solutions, Phys. Rev. B 82 (2010) 054115. doi:10.1103/PhysRevB.82.054115.

[38] S. Patinet, L. Proville, Depinning transition for a screw dislocation in a model solid solution, Phys. Rev. B 78 (2008) 104109. doi:10.1103/PhysRevB.78.104109.

[39] J. A. Yasi, L. G. Hector Jr, D. R. Trinkle, First-

principles data for solid-solution strengthening of magnesium: From geometry and chemistry to properties, Acta Mater. 58 (17) (2010) 5704 – 5713. doi:http://dx.doi.org/10.1016/j.actamat.2010.06.045.

[40] J. P. Hirth, J. Lothe, Theory of Dislocations, 2nd Edition, Wiley, New York, 1982.

[41] A. A. Hendrickson, M. E. Fine, Solid solution strengthening of Ag by Al, Trans. Metall. Soc. AIME 221 (5) (1961) 967–974.

[42] P. Jax, P. Kratochví, P. Haasen, Solid solution hardening of gold and other f.c.c. single crystals, Acta Metall. 18 (2) (1970) 237 – 245. doi:http://dx.doi.org/10.1016/0001-6160(70)90029-5.

[43] P. Kratochvíl, E. Neradová, Solid solution hardening in some copper based alloys, Czech. J. Phys. B 21 (12) (1971) 1273–1278. doi:10.1007/BF01699490.

[44] Z. Basinski, R. Foxall, R. Pascual, Stress equivalence of solution hardening, Scripta Metall. 6 (9) (1972) 807 – 814. doi:http://dx.doi.org/10.1016/0036-9748(72)90052-X.

[45] P. Haasen, P. Kratochví, in: Proceedings of the 3rd International Reinstoff-Symposium in Dresden, Akademie Verlag, Berlin, 1973, p. 383.

[46] Z. Trojanova, P. Haasen, Z. Metall. 60 (1975) 463.

[47] P. Haasen, in: F. R. N. Nabarro (Ed.), Dislocation in Solids, Vol. 4, North Holland, Amsterdam, 1979, p. 156.

[48] P. Haasen, Chapter 23 - mechanical properties of solid solutions, in: P. Haasen, R. W. Cahn (Eds.), Physical Metallurgy (4th, Revised and Enhanced Edition), 4th Edition, North-Holland, Oxford, 1996, pp. 2009 – 2073. doi:http://dx.doi.org/10.1016/B978-044489875-3/50028-4.

[49] B. J. Diak, Private comm.

[50] A. Argon, Thermally assisted motion of dislocations in solid solution-strengthened fcc alloys and the concept of "stress equivalence", Z. Metall. 95 (6) (2004) 406–410.

[51] T. Wille, W. Gieseke, C. Schwink, Quantitative analysis of solution hardening in selected copper alloys, Acta Metall. 35 (11) (1987) 2679 – 2693. doi:http://dx.doi.org/10.1016/0001-6160(87)90267-7.

[52] B. Diak, S. Saimoto, The determination of solute clusters in dilute aluminum alloys using strain rate sensitivity, Mater. Sci. Eng.: A 234–236 (1997) 1019 – 1022. doi:http://dx.doi.org/10.1016/S0921-5093(97)00342-0.

[53] B. Diak, K. Upadhyaya, S. Saimoto, Characterization of thermodynamic response by materials testing, Prog. Mater. Sci. 43 (4) (1998) 223 – 363. doi:http://dx.doi.org/10.1016/S0079-6425(98)00007-3.

[54] J. Zander, R. Sandström, L. Vitos, Modelling mechanical properties for non-hardenable aluminium alloys, Comp. Mat. Sci. 41 (1) (2007) 86 – 95. doi:http://dx.doi.org/10.1016/j.commatsci.2007.03.013.

[55] J. Zander, R. Sandström, One parameter model for strength properties of hardenable aluminium alloys, Mater. Des. 29 (8) (2008) 1540 – 1548. doi:http://dx.doi.org/10.1016/j.matdes.2008.02.001.

[56] D. Hull, D. J. Bacon, Introduction to Dislocations, 5th Edition, Butterworth-Heinemann, Oxford, UK, 2011.

[57] R. Labusch, Cooperative effects in alloy hardening, Czech. J. Phys. 38 (5) (1988) 474–481. doi:10.1007/BF01597457.

[58] M. Z. Butt, P. Feltham, Solid-solution hardening, J. Mater. Sci. 28 (1993) 2557–2576.

[59] M. Zaiser, Dislocation motion in a random solid solution, Philos. Mag. A 82 (15) (2002) 2869–2883. doi:doi:10.1080/01418610208240071.

[60] R. W. Smith, G. S. Was, Application of molecular dynamics to the study of hydrogen embrittlement in Ni-Cr-Fe alloys, Phys. Rev. B 40 (1989) 10322–10336. doi:10.1103/PhysRevB.40.10322.

[61] C. Varvenne, A. Luque, W. A. Curtin, Theory of solute strengthening for high entropy alloys, Acta Mater. 118 (2016) 164–176. doi:10.1016/j.actamat.2016.07.040.

[62] L. Nordheim, On the electronic structure of metals, Ann. Phys. 9 (1931) 607.

[63] R. J. Elliott, J. A. Krumhansl, P. L. Leath, The theory and properties of randomly disordered crystals and related physical systems, Rev. Mod. Phys. 46 (1974) 465–543. doi:10.1103/RevModPhys.46.465.

[64] F. Ducastelle, Order and Phase Stability in Alloys, North-Holland, Amsterdam, 1991.

[65] C. Varvenne, A. Luque, W. G. Nöhring, W. A. Curtin, Average-atom interatomic potentials for random alloys, Phys. Rev. B 93 (2016) 104201.

[66] S. I. Rao, C. Woodward, T. A. Parthasarathy, D. Dimiduk, D. B. Miracle, W. A. Curtin, Molecular statics and molecular dynamics simulations of dislocation behavior in model fcc and bcc multicomponent concentrated solid solution alloys, in preparation.

[67] R. Labusch, G. Grange, J. Ahearn, P. Haasen, Rate processes in plastic deformation of materials, in: J. C. M. Li, A. K. Mukherjee (Eds.), Proceedings from the John E. Dorn symposium, ASM, Metal Park, Ohio, 1975, p. 26.

[68] G. P. M. Leyson, W. A. Curtin, Solute strengthening at high temperatures, Modelling Simul. Mater. Sci. Eng. 24 (2016) 065005. doi:10.1088/09650393/24/065005.

[69] G. P. M. Leyson, W. A. Curtin, L. G. Hector Jr., C. Woodward, Quantitative prediction of solute strengthening in aluminium alloys, Nat. Mater. 9 (9) (2010) 750–755. doi:10.1038/NMAT2813.

[70] F. R. N. Nabarro, Thermally activated dislocation glide in moderately concentrated solid-solution, Philos. Mag. B 52 (3) (1985) 785–793. doi:10.1080/13642818508240636.

[71] I. Toda-Caraballo, P. E. J. Rivera-Díaz-del Castillo, Modelling solid solution hardening in high entropy alloys, Acta Mater. 85 (0) (2015) 14 – 23. doi:http://dx.doi.org/10.1016/j.actamat.2014.11.014.

[72] I. Toda-Caraballo, P. Rivera-Díaz-del Castillo, Modelling and design of magnesium and high entropy alloys through combining statistical and physical models, JOM 67 (1) (2015) 108–117. doi:10.1007/s11837-014-1242-2.

[73] X. Li, H. Zhang, S. Lu, W. Li, J. Zhao, B. Johansson, L. Vitos, Elastic properties of vanadium-based alloys from first-principles theory, Phys. Rev. B 86 (2012) 014105. doi:10.1103/PhysRevB.86.014105.

[74] D. B. Miracle, J. D. Miller, O. N. Senkov, C. Woodward, M. D. Uchic, J. Tiley, Exploration and development of high entropy alloys for structural applications, Entropy 16 (1) (2014) 494–525. doi:10.3390/e16010494.

[75] S. Vannarat, M. H. F. Sluiter, Y. Kawazoe, First-principles study of solute-dislocation interaction in

aluminum-rich alloys, Phys. Rev. B 64 (2001) 224203. doi:10.1103/PhysRevB.64.224203.
URL http://link.aps.org/doi/10.1103/PhysRevB.64.224203

[76] D. Ma, M. Friák, J. von Pezold, D. Raabe, J. Neugebauer, Computationally efficient and quantitatively accurate multiscale simulation of solid-solution strengthening by ab initio calculation, Acta Mater. 85 (2015) 53 – 66. doi:http://dx.doi.org/10.1016/j.actamat.2014.10.044.

[77] C. Varvenne, O. Mackain, L. Proville, E. Clouet, Hydrogen and vacancy clustering in zirconium, Acta Mater. 102 (2016) 56 – 69. doi:http://dx.doi.org/10.1016/j.actamat.2015.09.019.

[78] M. Ghazisaeidi, D. R. Trinkle, Interaction of oxygen interstitials with lattice faults in Ti, Acta Materialia 76 (2014) 82–86.

[79] S. A. Kibey, L. L. Wang, J. B. Liu, H. T. Johnson, H. Sehitoglu, D. D. Johnson, Quantitative prediction of twinning stress in fcc alloys: Application to Cu-Al, Phys. Rev. B 79 (2009) 214202.

[80] A. Abbasi, A. Dick, T. Hickel, J. Neugebauer, First-principles investigation of the effect of carbon on the stacking fault energy of Fe-C alloys, Acta Mater. 59 (8) (2011) 3041–3048. doi:10.1016/j.actamat.2011.01.044.

[81] C. Woodward, D. R. Trinkle, L. G. Hector Jr., D. L. Olmsted, Prediction of dislocation cores in aluminum from density functional theory, Phys. Rev. Lett. 100 (2008) 045507. doi:10.1103/PhysRevLett.100.045507.

[82] D. L. Olmsted, L. G. Hector Jr, W. A. Curtin, Molecular dynamics study of solute strengthening in Al/Mg alloys, J. Mech. Phys. Solids 54 (2006) 1763–1788. doi:10.1016/j.jmps.2005.12.008.

[83] B. A. Szajewski, F. Pavia, Y. Dong, W. A. Curtin, Robust line tension via atomistics, Modelling Simul. Mater. Sci. Eng. 23 (8) (2015) 085008.

[84] A. Akhtar, A. Teghtsoonian, Substitional solution hardening of magnesium single-crystals, Philos. Mag. 25 (4) (1972) 897–&. doi:10.1080/14786437208229311.

[85] K. Marukawa, A new model of solution hardening in fcc metals based on the interaction with plural obstacles, Philos. Mag. 87 (26) (2007) 4027–4046. doi:10.1080/14786430701481756.

[86] M. Ghazisaeidi, L. G. Hector Jr, W. A. Curtin, Solute strengthening of twinning dislocations in Mg alloys, Acta Mater. 80 (2014) 278 – 287. doi:http://dx.doi.org/10.1016/j.actamat.2014.07.045.

[87] X.-Y. Liu, J. B. Adams, F. Ercolessi, J. A. Moriarty, EAM potential for magnesium from quantum mechanical forces, Modelling Simul. Mater. Sci. Eng. 4 (3) (1996) 293.

[88] M. Ghazisaeidi, W. A. Curtin, Analysis of dissociation of $\langle c \rangle$ and $\langle c+a \rangle$ dislocations to nucleate $(1\,0\,\bar{1}\,2)$ twins in Mg, Modelling Simul. Mater. Sci. Eng. 21 (5) (2013) 055007.

[89] E. W. Kelly, W. F. Hosford Jr, Deformation characteristics of textured magnesium, Trans. AIME 242 (4) (1968) 654.

[90] N. Stanford, M. R. Barnett, Solute strengthening of prismatic slip, basal slip and twinning in Mg and Mg–Zn binary alloys, Int. J. Plasticity 47 (2013) 165 – 181. doi:http://dx.doi.org/10.1016/j.ijplas.2013.01.012.

[91] M. R. Barnett, Z. Keshavarz, A. G. Beer, D. Atwell, Influence of grain size on the compressive deformation of wrought mg–3al–1zn, Acta Mater. 52 (17) (2004) 5093 – 5103. doi:http://dx.doi.org/10.1016/j.actamat.2004.07.015.

[92] J. Bohlen, P. Dobroň, J. Swiostek, D. Letzig, F. Chmelík, P. Lukáč, K. U. Kainer, On the influence of the grain size and solute content on the {AE} response of magnesium alloys tested in tension and compression, Mater. Sci. Eng. A 462 (1–2) (2007) 302 – 306, international Symposium on Physics of Materials, 2005. doi:http://dx.doi.org/10.1016/j.msea.2006.02.470.

[93] L. Chang, Y. Wang, X. Zhao, M. Qi, Grain size and texture effect on compression behavior of hot-extruded Mg–3Al–1Zn alloys at room temperature, Mater. Charact. 60 (9) (2009) 991 – 994. doi:http://dx.doi.org/10.1016/j.matchar.2009.04.001.

[94] D. L. Yin, J. T. Wang, J. Q. Liu, X. Zhao, On tension–compression yield asymmetry in an extruded Mg–3Al–1Zn alloy, J. Alloys Compd. 478 (1–2) (2009) 789 – 795. doi:http://dx.doi.org/10.1016/j.jallcom.2008.12.033.

[95] M. Barnett, M. Setty, F. Siska, Estimating critical stresses required for twin growth in a magnesium alloy, Metall. Mater. Trans. A 44 (7) (2013) 2962–2969. doi:10.1007/s11661-012-1573-y.

[96] Z. Wu, Y. Gao, H. Bei, Thermal activation and labusch-type strengthening analysis for a family of high-entropy and equiatomic solid-solution alloys, Acta Mater. 120 (2016) 108–119. doi:http://dx.doi.org/10.1016/j.actamat.2016.08.047.

[97] Z. Wu, H. Bei, G. Pharr, E. George, Temperature dependence of the mechanical properties of equiatomic solid solution alloys with face-centered cubic crystal structures, Acta Mater. 81 (0) (2014) 428 – 441. doi:http://dx.doi.org/10.1016/j.actamat.2014.08.026.

[98] Z. Wu, H. Bei, F. Otto, G. Pharr, E. George, Recovery, recrystallization, grain growth and phase stability of a family of fcc-structured multi-component equiatomic solid solution alloys, Intermetallics 46 (0) (2014) 131 – 140. doi:http://dx.doi.org/10.1016/j.intermet.2013.10.024.

[99] F. Otto, A. Dlouhý, C. Somsen, H. Bei, G. Eggeler, E. George, The influences of temperature and microstructure on the tensile properties of a CoCrFeMnNi high-entropy alloy, Acta Mater. 61 (15) (2013) 5743 – 5755. doi:http://dx.doi.org/10.1016/j.actamat.2013.06.018.

[100] F. Abe, T. Tanabe, Change in lattice spacing of nickel by dissolved chromium and tungsten, Z. Metall. 76 (6) (1985) 420–425.

[101] J. Bandyopadhyay, K. P. Gupta, Low temperature lattice parameter of nickel and some nickel-cobalt alloys and grüneisen parameter of nickel, Cryogenics (1977) 345–347.

[102] A. J. Zaddach, C. Niu, C. C. Koch, D. L. Irving, Mechanical properties and stacking fault energies of NiFeCrCoMn high-entropy alloy, JOM 65 (12) (2013) 1780–1789. doi:10.1007/s11837-013-0771-4.

[103] S. Huang, W. Li, S. Lu, F. Tian, J. Shen, E. Holmstrom, L. Vitos, Temperature dependant stacking fault energy of FeCrCoNiMn high entropy alloy, Scripta

Mater. 108 (2015) 44–47. doi:10.1016/j.scriptamat.2015.05.041.

[104] T. M. Smith, M. S. Hooshmand, B. D. Esser, F. Otto, D. W. McComb, E. P. George, M. Ghazisaeidi, M. J. Mills, Atomic-scale characterization and modeling of 60° dislocations in a high-entropy alloy, Acta Mater. 110 (2016) 352–363.

[105] L. Proville, L. Ventelon, D. Rodney, Prediction of the kink-pair formation enthalpy on screw dislocations in α-iron by a line tension model parameterized on empirical potentials and first-principles calculations, Phys. Rev. B 87 (2013) 144106. doi:10.1103/PhysRevB.87.144106.

[106] D. D. Johnson, D. M. Nicholson, F. J. Pinski, B. L. Gyorffy, G. M. Stocks, Density-functional theory for random alloys: Total energy within the coherent-potential approximation, Phys. Rev. Lett. 56 (1986) 2088–2091. doi:10.1103/PhysRevLett.56.2088.

[107] D. D. Johnson, M. Asta, Energetics of homogeneously-random fcc Al-Ag alloys: A detailed comparison of computational methods, Comput. Mater. Sci. 8 (1–2) (1997) 54 – 63, proceedings of the joint NSF/CNRS Workshop on Alloy Theory. doi:http://dx.doi.org/10.1016/S0927-0256(97)00016-5.

[108] C. A. Johnson, The growth of prismatic dislocation loops during annealing, Philos. Mag. 5 (1960) 1255–1265. doi:10.1080/14786436008238338.

[109] A. Zunger, S.-H. Wei, L. G. Ferreira, J. E. Bernard, Special quasirandom structures, Phys. Rev. Lett. 65 (1990) 353–356. doi:10.1103/PhysRevLett.65.353.

[110] J. von Pezold, A. Dick, M. Friák, J. Neugebauer, Generation and performance of special quasirandom structures for studying the elastic properties of random alloys: Application to Al-Ti, Phys. Rev. B 81 (2010) 094203. doi:10.1103/PhysRevB.81.094203.

[111] S. Patinet, L. Proville, Dislocation pinning by substitutional impurities in an atomic-scale model for Al(Mg) solid solutions, Philos. Mag. 91 (11) (2011) 1581–1606. doi:10.1080/14786435.2010.543649.

[112] A. Tehranchi, W. A. Curtin, Softening and hardening of yield stress by hydrogen-solute interactions, submitted.

[113] D. R. Trinkle, C. Woodward, The chemistry of deformation: How solutes soften pure metals, Science 310 (2005) 1665–1667. doi:10.1126/science.1118616.

[114] G. Bonny, D. Terentyev, R. C. Pasianot, S. Ponce, A. Bakaev, Interatomic potential to study plasticity in stainless steels: the FeNiCr model alloy, Modelling Simul. Mater. Sci. Eng. 19 (8). doi:10.1088/0965-0393/19/8/085008.

[115] L. Proville, D. Rodney, Y. Bréchet, G. Martin, Atomic-scale study of dislocation glide in a model solid solution, Philos. Mag. 86 (2006) 3893–3920. doi:10.1080/14786430600567721.

[116] P. Yi, R. C. Cammarata, M. L. Falk, Atomistic simulation of solid solution hardening in mg/al alloys: Examination of composition scaling and thermo-mechanical relationships, Acta Materialia 105 (2016) 378 – 389. doi:http://dx.doi.org/10.1016/j.actamat.2015.12.038.
URL http://www.sciencedirect.com/science/article/pii/S1359645415301440

[117] T. Nogaret, D. Rodney, Finite-size effects in dislocation glide through random arrays of obstacles: Line tension simulations, Phys. Rev. B 74 (2006) 134110. doi:10.1103/PhysRevB.74.134110.
URL http://link.aps.org/doi/10.1103/PhysRevB.74.134110

[118] C. Niu, A. J. Zaddach, A. A. Oni, X. Sang, J. W. Hurt, J. M. LeBeau, C. C. Koch, D. L. Irving, Spin-driven ordering of Cr in the equiatomic high entropy alloy NiFeCrCo, Appl. Phys. Lett. 106 (16). doi:http://dx.doi.org/10.1063/1.4918996.

[119] M. Jouiad, F. Pettinari-Sturmel, N. Clement, A. Coujou, Dynamic friction in the γ phase of a nickel-based superalloy, Philos. Mag. 79 (11) (1999) 2591–2602.

[120] A. T. Adorno, W. Garlipp, M. Cilense, R. A. G. Silva, Order-disorder transformation in the Ni-4.49 at.(2006) 55–59. doi:10.1016/j.jallcom.2005.07.020.

[121] F. Pettinari-Sturmel, M. Jouiad, H. O. K. Kirchner, N. Clement, A. Coujou, Local disordering and reordering phenomena induced by mobile dislocations in short-range-ordered solid solutions, Philos. Mag. 82 (16) (2002) 3045–3054. doi:10.1080/01418610210161602.

[122] J. Fisher, On the strength of solid solution alloys, Acta Metall. 2 (1) (1954) 9–10. doi:http://dx.doi.org/10.1016/0001-6160(54)90087-5.

[123] A. de Vaucorbeil, C. W. Sinclair, W. J. Poole, Dislocation glide through non-randomly distributed point obstacles, Philos. Mag. 93 (27) (2013) 3664–3679. doi:10.1080/14786435.2013.820384.